Transonic Aeroelastic Stability Analysis Using a Kriging–Based Schur Complement Formulation

S. Timme*, S. Marques† and K. J. Badcock‡

CFD Laboratory, University of Liverpool, Liverpool L63 3GH, United Kingdom

An efficient approach is presented to search for transonic aeroelastic instability of realistic aircraft structures in multidimensional parameter spaces. Aeroelastic instability is predicted by a small nonlinear eigenvalue problem for the structural equations which is corrected by the aerodynamic influence. The approximation of this computationally expensive interaction term, simulated by nonlinear high fidelity computational fluid dynamics, is formulated to allow both the blind search for aeroelastic instability and the update of lower order predictions with available better information. The approximation is based on a kriging interpolation of exact numerical samples covering the parameter space. The approach is presented for the Goland and MDO wing configurations and the open source fighter.

I. Introduction

The fast prediction of aeroelastic instability is an important engineering challenge in aircraft design and certification. Standard approaches in industrial applications to determine the aeroelastic stability of an aircraft structure are the classical k or p–k methods [1]. These use an inviscid linearised theory in the frequency domain to determine the unsteady aerodynamic response. Here, the doublet lattice method has been the single most important tool in large scale production flutter analyses for more than 30 years [2]. Modern aircraft routinely operate in the transonic regime with its mixed sub- and supersonic regions where a linear aerodynamic theory fails due to the presence of flow nonlinearities such as shock waves and shock induced flow separation. The linear numerical predictions have to be corrected with data from experimental campaigns or higher fidelity flow simulations [3, 4].

The transonic aerodynamics have to be modelled by nonlinear methods for satisfactory and accurate results [5]. The use of computational aeroelasticity employing high fidelity aerodynamics based on nonlinear computational fluid dynamics (CFD) has matured from a research exercise to a powerful tool in engineering applications due to advances in algorithms and computer power over the last four decades [6]. The stability of an aeroelastic system can be inferred from time–accurate simulations following an initial excitation [7, 8]. This approach is very capable due to its generality in dealing with dynamically nonlinear systems, while the significant cost of CFD–based simulations to solve for the unsteady, nonlinear transonic aerodynamics is a major drawback, thus limiting the analysis to a few carefully chosen cases. This is exacerbated by the requirement to search a space of system parameters and flight conditions for critical conditions.

To obviate the cost involved in solving complex systems with millions of degrees–of–freedom, and to permit routine calculations over the flight envelope, alternative approaches have been investigated over the last decade. There are two distinct directions. One direction, referred to as reduced order modelling, extracts the essence of the dynamic aeroelastic system to form a low dimensional problem while trying to keep the accuracy of the full order formulation. Popular approaches are proper orthogonal decomposition [9–11] and system identification based on the Volterra theory [12, 13]. The second direction keeps the (spatial) order of the full system while manipulating its solution procedure to reduce the cost. One popular approach is the harmonic balance method [14, 15] giving a reduction in the computational cost associated

*Research Associate, School of Engineering. email: Sebastian.Timme@liverpool.ac.uk, Member AIAA

†Research Associate, School of Engineering. email: S.Marques@liverpool.ac.uk, Member AIAA

‡Professor, School of Engineering. email: K.J.Badcock@liverpool.ac.uk, Senior Member AIAA

with simulating dynamically nonlinear, time–periodic, unsteady problems such as limit–cycle oscillation. Another one, presented in this work, uses the theory of dynamical systems to predict aeroelastic instability of the Hopf type commonly leading to flutter or limit–cycle oscillation. Here, a (linear) stability problem for a (nonlinear) steady state solution of the aeroelastic system is examined instead of performing unsteady simulations.

Following an approach first published in [16, 17], the bifurcation method, solving an augmented system of equations for the bifurcation point defining the onset of the aeroelastic instability, was successfully tested on a pitch–and–plunge aerofoil configuration and the flexible AGARD 445.6 wing [18, 19]. However, the CFD–based aeroelastic system is typically large making it difficult to solve the augmented system for the bifurcation point directly. Consequently, several major development steps have taken place since this early work to ease the simulations.

First, the shifted inverse power method was adapted to allow the tracing of the aeroelastic modes, starting out in the wind–off structural system and typically defining the instability, with changing values of the independent system parameter, i.e. a representation of the dynamic pressure. This provides information about the damping and frequency of the aeroelastic modes [20]. Secondly, an improved version of the basic method used the Schur complement eigenvalue formulation for enhanced computational performance while avoiding numerical problems associated with the shifted inverse power method [21]. It was applied to several wing structures and also complete aircraft configurations [22,23]. This approach views the coupled aeroelastic system as a modified structural eigenvalue problem with the interaction term, which depends on the response frequency and the parameters defining the steady state solution, correcting for the aerodynamic influence. The evaluation of the interaction term incurs most of the involved cost as it generally requires operations on the high dimensional CFD–based system.

Thirdly, the approximation of this interaction term was formulated (for aerofoil cases) to search parameter spaces for aeroelastic instability and to exploit a hierarchy of nonlinear aerodynamic models, with cheaper models being used to evaluate possible conditions of interest for more expensive models, whose evaluation is then used to update the approximation [24]. The approximation of the interaction term, using kriging interpolation based on true numerical samples covering the parameter space of interest, made the Schur complement eigenvalue method essentially a reduced order model with the unmodified full order fluid response projected onto the structural system. This projection of the exact fluid response is different to, for instance, the aerodynamic representation when using proper orthogonal decomposition. Alternative interpolation techniques have been discussed to do the task of reconstruction [25]. This paper extends the ideas associated with reconstructing the interaction matrix to three dimensional test cases under matched conditions.

The paper continues with the details of the aeroelastic stability analysis. The aerodynamic and structural models used are described, and the Schur complement eigenvalue method including the generation and approximation of the interaction matrix is outlined. Then, the aeroelastic stability analyses for the Goland and MDO wings as well as a generic fighter aircraft are presented to illustrate the approach.

II. Eigenvalue Stability Formulation

A. Flow Models

In the current paper, the Euler and Reynolds–averaged Navier–Stokes (RANS) equations are used as the aerodynamic models. The governing equations are solved using an established research code [26]. The code uses a block–structured, cell–centred, finite–volume scheme for spatial discretisation. Convective fluxes are evaluated by the approximate Riemann solver of Osher and Chakravarthy [27] with the MUSCL scheme [28] achieving essentially second order accuracy and van Albada's limiter preventing spurious oscillations around steep gradients. Viscous fluxes are evaluated by central differences. Linear eddy viscosity turbulence models considered in this work are solved in a fashion similar to the RANS equations with source terms being evaluated at cell centres. Boundary conditions are enforced using two layers of halo cells.

Spatial discretisation leads to a system of n_f first order ordinary differential equations in time written in semidiscrete state–space representation as $\dot{\boldsymbol{w}}_f = \boldsymbol{R}_f(\boldsymbol{w}_f, \boldsymbol{w}_s)$ where $\boldsymbol{w}$ denotes vectors of unknowns and $\boldsymbol{R}_f$ is the fluid residual vector. The subscripts f and s denote fluid and structural contributions, respectively, with the latter contribution influencing the fluid response due to the moving fluid mesh in unsteady simulations. Implicit time marching converges to steady state solutions, while a second order dual time stepping is used for unsteady simulations [29]. Resulting linear systems are solved by a preconditioned Krylov subspace iterative method.

B. Modal Structural Model

As is common in computational aeroelasticity, an aircraft structure is represented by a small number of normal modes, small compared with the large dimension of the CFD system. The deflections $\delta\boldsymbol{x}_s$ of the structure are defined at a set of points $\boldsymbol{x}_s$ by $\delta\boldsymbol{x}_s(t) = \Phi(\boldsymbol{x}_s)\,\boldsymbol{\eta}(t)$, where the vector $\boldsymbol{\eta}$ contains the n generalised coordinates (modal amplitudes). The columns of the matrix Φ contain the mode shape vectors evaluated from a finite–element model of the structure using the commercial software package MSC.Nastran. The finite–element equations are projected onto the mode shapes and an appropriate scaling is applied to obtain generalised masses of magnitude one according to $\Phi^T M \Phi = I$. A system of $2n$ scalar equations is given for the modal structural model in state–space representation, denoted here as $\dot{\boldsymbol{w}}_s = \boldsymbol{R}_s(\boldsymbol{w}_f, \boldsymbol{w}_s)$, with $\boldsymbol{w}_s = [\,\boldsymbol{\eta}, \dot{\boldsymbol{\eta}}\,]^T$ containing the generalised coordinates and their velocities. The corresponding residual vector, neglecting structural damping, is written as $\boldsymbol{R}_s = D\,\boldsymbol{w}_s + \mu\,E\,\Phi^T\boldsymbol{f}(\boldsymbol{w}_f, \boldsymbol{w}_s)$, with the matrices $D = [0, I; -\Phi^T K \Phi, 0]$ and $E = [0, I]^T$, where I is the $n \times n$ identity matrix. The generalised stiffness matrix $\Phi^T K \Phi$ contains the n normal mode frequencies squared on the diagonal. The vector $\boldsymbol{f}$ of aerodynamic forces at the structural grid points follows from the wall pressure, the area of the surface segment and the unit normal vector. The independent (bifurcation) parameter μ is obtained from the nondimensionalisation of the governing equations and depends on the altitude.

In the common situation, the structural grid points $\boldsymbol{x}_s$ not only do not conform with the aerodynamic surface grid, but are also defined on different surfaces. This requires the transfer of information between the fluid and structural grids. The aerodynamic (pressure) forces, defined at the surface grid, have to be transferred to the structural grid, and the modal deflections $\delta\boldsymbol{x}_s$ have to be communicated back to the CFD surface mesh. This is achieved using a method called the constant volume tetrahedron transformation [30]. Also, different to a rigid aerofoil formulation, the geometry of interest (and thus the computational mesh) deforms. This is achieved using a transfinite interpolation of the surface displacements to the internal grid points [26].

The evaluation of the Jacobian matrix blocks is required for the eigenvalue–based stability analysis. The matrix A_{ss} is conveniently split into two contributions; one from the normal mode frequencies and one due to the aerodynamic force vector. It is given by $A_{ss} = D + \mu\,E\,\Phi^T \partial\boldsymbol{f}/\partial\boldsymbol{w}_s$. The second term is usually negligible. The Jacobian matrix block A_{sf} describes how the structure responds to changes in the flow field and is formed as $A_{sf} = \mu\,E\,\Phi^T \partial\boldsymbol{f}/\partial\boldsymbol{w}_f$. Currently, the evaluation of the derivatives $\partial\boldsymbol{f}/\partial\boldsymbol{w}_s$ and $\partial\boldsymbol{f}/\partial\boldsymbol{w}_f$ is done using finite differences. Conveniently, the bifurcation parameter is set to unity for the evaluation of the Jacobian matrices and adjusted in a matched fashion once needed as discussed in the following.

C. Schur Complement Eigenvalue Method

The aeroelastic system is written in state–space form as $\dot{\boldsymbol{w}} = \boldsymbol{R}(\boldsymbol{w}, \mu)$, with the vectors of unknowns $\boldsymbol{w}$ and corresponding residuals $\boldsymbol{R}$ containing fluid and structural contributions. The parameter μ is the bifurcation parameter representing the dynamic pressure for the aeroelastic simulations. The expression $\boldsymbol{R}(\boldsymbol{w}_0, \mu) = 0$ is satisfied by an equilibrium solution $\boldsymbol{w}_0$ of the nonlinear system. Stability is determined by eigenvalues $\lambda = \sigma \pm i\omega$ of the system Jacobian matrix $A(\boldsymbol{w}_0, \mu)$ evaluated at the steady state and chosen values of μ. Importantly, the Jacobian matrix is exact with respect to the applied spatial discretisation scheme. A stable system has all its eigenvalues with a negative real part. In many aeroelastic problems a pair of complex conjugate eigenvalues with zero real part defines the onset of an instability of the Hopf type leading to flutter and limit–cycle oscillation.

Linear aeroelastic stability is predicted by solving the standard eigenvalue problem, $(A - \lambda I)\,\boldsymbol{p} = 0$, where the Jacobian matrix is conveniently partitioned in blocks expressing the different dependencies

$$A = \frac{\partial \boldsymbol{R}}{\partial \boldsymbol{w}} = \begin{pmatrix} A_{ff} & A_{fs} \\ A_{sf} & A_{ss} \end{pmatrix}. \tag{1}$$

Writing the eigenvector $\boldsymbol{p}$ just as the vector of unknowns in fluid and structural contributions, the Schur complement eigenvalue method [31] can be given. The expression $S(\lambda)\,\boldsymbol{p}_s = 0$ defines a small nonlinear eigenvalue problem for the stability analysis with the Schur complement matrix $S(\lambda)$ explicitly written as,

$$S(\lambda) = (A_{ss} - \lambda I) - A_{sf}\,(A_{ff} - \lambda I)^{-1} A_{fs}, \tag{2}$$

where λ is an eigenvalue of the structural part in the uncoupled system. The first term on the right–hand

side, denoted as $S^s = A_{ss} - \lambda I$, defines the structural eigenvalue problem, while the second part describes the interaction (coupling) term, $S^c = -A_{sf}\,(A_{ff} - \lambda I)^{-1} A_{fs}$.

To solve this small complex–valued eigenvalue problem, the system is augmented to scale the structural eigenvector $\boldsymbol{p}_s$ against a real–valued constant vector $\boldsymbol{c}_s$, i.e. augment by the expression $\boldsymbol{c}_s^T \boldsymbol{p}_s - i = 0$ which is an arbitrary choice. Then, the augmented nonlinear system of the Schur residual is solved for the unknowns $\left[\boldsymbol{p}_s, \lambda\right]^T$. While the full eigenvalue formulation solves a problem with $n_f + 2n + 1$ unknowns, the Schur complement formulation only has $2n + 1$ where the number n of relevant normal modes is generally small. Ways to evaluate the roots of the Schur residual are outlined in the following.

An efficient way of finding the roots of nonlinear systems are Newton methods which require forming the residual and its Jacobian matrix (or an approximation). The evaluation of the interaction term S^c is the main cost in either method since it involves operations on the high dimensional fluid system, whereas the cost to form the structural term S^s is negligible in comparison. Using Newton's method, the interaction term in the Schur residual is conveniently evaluated by first forming the product $A_{fs}\,\boldsymbol{p}_s$ for the current approximation to the eigenvector, and then solving one linear system, $(A_{ff} - \lambda I)\,\boldsymbol{y} = A_{fs}\,\boldsymbol{p}_s$, the solution of which is multiplied against the matrix A_{sf}. Applying finite differences gives the Schur Jacobian matrix where multiple evaluations of the residual are required.

As there are n relevant solutions of the nonlinear eigenvalue problem, the cost of forming the interaction term at each Newton iteration, for each value of the independent parameter, and for a range of system parameters becomes too high without approximations. Thus, a series approximation [32] of the Schur complement matrix can be written for $\lambda = \lambda_0 + \lambda_\varepsilon$ as

$$S(\lambda) \approx (A_{ss} - \lambda I) - A_{sf} \left(\left(A_{ff} - \lambda_0 I\right)^{-1} + \lambda_\varepsilon \left(A_{ff} - \lambda_0 I\right)^{-2} \right) A_{fs}, \tag{3}$$

where λ_ε denotes a small variation to the reference value λ_0, which is, for instance, a structural frequency or a previously converged solution. Pre–computing the factors in the series against the matrix A_{fs} (requiring $4n$ linear solves per shift λ_0 for the first order expansion), allows the application of the expansion in the vicinity of λ_0. Two approaches have been discussed [22,31]. The quasi–Newton method evaluates the (exact) residual by the nonlinear approach given in the previous paragraph, while the series expansion is used for the Schur Jacobian matrix. The series method also applies the series expansion to the residual which is possible for small λ_ε and for an independent parameter μ not affecting the pre–computed values, i.e. for symmetric problems.

The big computational challenge in solving the small nonlinear eigenvalue problem is the evaluation of the Schur interaction matrix S^c to form the Schur residual and Jacobian matrix as this involves operations on the high dimensional CFD–based fluid system. This matrix depends on the eigenvalue, particularly the imaginary part, and the steady state solution. The steady state makes it dependent on a large number of parameters in both the flow model, e.g. Mach number, angle of attack and dynamic pressure, and the structural model due to structural parameters generally affecting the mode shapes. This means that the direct evaluation of the matrix S^c (using either of the three described approaches) will become too expensive if a large space of system parameters has to be searched for aeroelastic instability.

For computationally expensive simulations, such as the generation of the Schur interaction matrix, it is useful to generate a cheap approximation based on relatively few runs of the expensive full order model to provide information about its response at untried parameter combinations. An approximation model should both predict the calculated responses precisely and adapt to the functional behaviour of the responses. Several approaches to construct response surfaces can be found in the literature. In this study, as introduced in [24], the Schur interaction matrix is reconstructed based on samples, i.e. full order evaluations of this term covering the parameter space of interest, using the kriging interpolation technique. Once the interaction matrix can be represented by the kriging model, the eigenvalue problem can be solved as often as necessary at very low computational cost using any of the above three approaches.

Approximating the Schur Interaction Matrix: Extracting Samples

The interaction matrix can be formed in both the frequency and time domain. Solving $2n$ linear systems of the form $(A_{ff} - \lambda I)\,\boldsymbol{y} = A_{fs}$ directly (one for each structural unknown of the state–space representation corresponding to the columns of the matrix A_{fs}) and multiplying the solution by the matrix A_{sf} to form the Schur interaction matrix is referred to as the (first) linear frequency domain approach. This follows the original implementation of the eigenvalue solver [31].

Importantly, the matrix A_{fs} can be written as $A_{fs} = [A_{f\eta}, A_{f\dot{\eta}}]$ to illustrate the dependence of the fluid residual $\boldsymbol{R}_f(\boldsymbol{w}_f, \boldsymbol{x}, \dot{\boldsymbol{x}})$ on the structural unknowns $\boldsymbol{w}_s = [\boldsymbol{\eta}, \dot{\boldsymbol{\eta}}]$ with generalised coordinates $\boldsymbol{\eta}$ and their velocities $\dot{\boldsymbol{\eta}}$ influencing the grid displacements $\boldsymbol{x}(\boldsymbol{\eta})$ and grid velocities $\dot{\boldsymbol{x}}(\dot{\boldsymbol{\eta}})$ of the fluid mesh. Then, the above relation for the first approach can be rearranged as $(A_{ff} - \lambda I)\,\boldsymbol{y} = (A_{f\eta} + \lambda A_{f\dot{\eta}})$ to solve half the number of linear systems, one for each of the n structural degrees–of–freedom[a]. This relation can be seen by observing that for the state–space representation the structural eigenvector is written as $\boldsymbol{p}_s = [\boldsymbol{p}_\eta, \lambda\,\boldsymbol{p}_\eta]^T$ using the expression $\boldsymbol{\eta} = \boldsymbol{p}_\eta\, e^{\lambda t}$ consistent with a linear stability analysis [33]. The alternative is referred to as the second approach. Either approach in the frequency domain is a preferred choice due to the significant computational cost involved in time domain simulations.

Alternatively in the time domain, the interaction matrix (i.e. the aerodynamic influence coefficient matrix) is evaluated from the generalised forces $\Phi^T \boldsymbol{f}$ following an excitation in the structural unknowns. When applied in the current study, one structural degree–of–freedom at a time is excited in a forced sinusoidal motion at a fundamental frequency of $\lambda = i\,\omega$ applying a physically meaningful and mathematically consistent relation between deflection and deflection rate. The generalised forces are Fourier decomposed and divided by the corresponding Fourier coefficient of the forced structural motion. More elegant and efficient approaches to evaluate the aerodynamic influence from unsteady CFD–based simulations over a range of frequencies can be used, such as an exponentially–shaped pulse excitation [34] or unit step/impulse excitation [13,35]. However, this is not needed as the kriging interpolation technique is applied instead.

Approximating the Schur Interaction Matrix: Kriging Interpolation

An excellent description on the background to the kriging approach was given in [36]. Herein only a very brief overview is provided. In the kriging interpolation technique a multidimensional deterministic response of a simulation is treated as a realisation of a stochastic process. This process is composed of a low order regression model and a random normally distributed signal with zero mean and a covariance depending on the variance of the input samples and the correlation between two parameter locations. Thus, the second term (the error term) is not independent at different locations but is related to the distance between points in the parameter space. The parameters of the computationally cheap kriging model are determined for a known set of (typically expensive) numerical samples of the full order formulation by an optimisation process as given, for instance, in [36, 37]. Importantly, the kriging predictor gives the exact system response at a sampled location.

III. Application to Aeroelastic Stability Analysis

A. Goland Wing – Symmetric Case without Aerostatic Effects

First, the problem without aerostatic deformation is considered. Conveniently, write the Schur complement matrix S in Eq. (2) as

$$S = (C_1 + \mu\, C_2 - \lambda I\,) - \mu\, C_3\,(A_{ff} - \lambda I)^{-1} A_{fs} \tag{4}$$

where the matrices C_1, C_2 and C_3 follow directly from the equations of the matrices A_{ss} and A_{sf} given in the previous section. This form allows the evaluation of the matrices C_2 and C_3 independently from the bifurcation parameter μ, typically representing the dynamic pressure. The matrices A_{ff} and A_{fs} contain sensitivities of the fluid system which is, by default, made dimensionless by freestream reference values making these matrices independent of altitude. This formulation is possible since, at this point, aerostatic effects are not considered.

The construction of the approximation model without aerostatic effects is simplified in the sense that a matched simulation only requires the adjustment of the independent parameter to the current value of the reference density. The other part of the computationally expensive interaction term, $\widetilde{S}^c = -C_3\,(A_{ff} - \lambda I)^{-1} A_{fs}$, is sampled for different values of the eigenvalue and freestream Mach number. The matrix $C_1 = D$ also needs to be matched to the current reference values as the normal mode frequencies are made dimensionless using the reference freestream velocity. However, this task is trivial. The matrix C_2,

[a]Note that the same rearrangement can be applied to Eqs. (2) and (3) when using the exact eigenvalue solver. However, this does not result in a cost reduction as the required number of linear solves remains unchanged. For instance, the evaluation of the alternative factors for the series method still requires $4n$ linear solves as the right–hand side would be changed according to $(A_{f\eta} + \lambda_0 A_{f\dot{\eta}}) + \lambda_\varepsilon A_{f\dot{\eta}}$. This is therefore not further pursued for the exact eigenvalue solver, while it is a very useful observation for the sample extraction.

containing the sensitivities of the force vector with respect to the deformation, is neglected, similar to the aerofoil formulation [24], as it was found to be several (typically 3 to 5) orders of magnitude smaller than the other terms. Indeed, the reconstruction of the interaction term is considered as the most significant source of error.

Thus, the approximated Schur complement matrix used for the stability analysis is written as

$$S = \widetilde{S}^s(\lambda, h_r, M_r) + \mu(h_r, M_r)\,\widehat{S}^c(\omega, M_r) \tag{5}$$

where the variable h_r indicates the dependence on the altitude in addition to the freestream Mach number M_r. The matrix $\widetilde{S}^s = C_1 - \lambda I$ is the modified structural term excluding the dependence on the force vector and $\widehat{S}^c$ is the kriging prediction of the modified interaction term $\widetilde{S}^c$ excluding the bifurcation parameter. Then, the roots of the approximated Schur residual are found by any Newton method. In the first instance, the interaction term is evaluated for an eigenvalue with zero real part, as discussed in the aerofoil study [24], while the structural part uses the complete eigenvalue making it an analogy to the classical p–k method. This simplification is appropriate for the modal structural model as will be seen in the following discussion. Using the formulation in Eq. (5), the approaches of sampling and kriging for the matched simulations using a modal structural model become equivalent to the previous aerofoil study with only minor modifications. The approach is applied in the following.

Different types of matched simulations are discussed. First, an altitude can be chosen to set the reference value of the density, influencing the bifurcation parameter μ, and then the freestream velocity, only influencing the matrix C_1 through nondimensionalisation, is varied to detect the onset of the instability. Secondly, the altitude can be varied independently while adjusting the values of the density and speed of sound according to the standard atmosphere conditions. Then, the velocity follows from the current Mach number. The latter approach is mainly used herein.

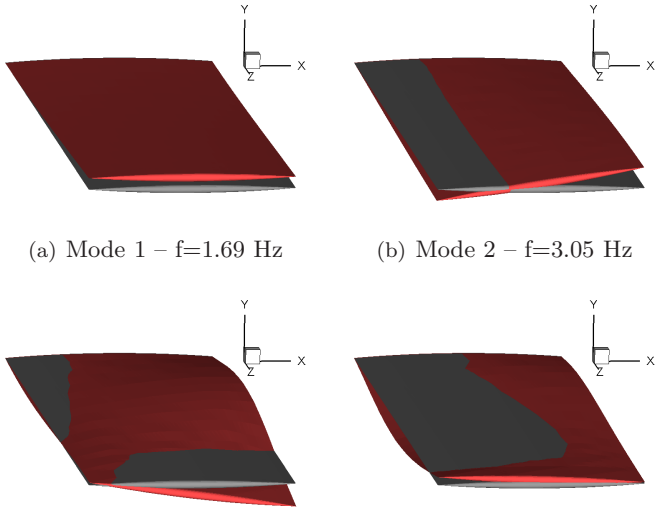

(a) Mode 1 – f=1.69 Hz (b) Mode 2 – f=3.05 Hz

(c) Mode 3 – f=9.17 Hz (d) Mode 4 – f=10.8 Hz

Figure 1. Mode shapes of Goland wing/store configuration.

The Goland wing is a model wing having a chord of 1.8266 m and a span of 6.096 m. It is rectangular and cantilevered with a constant cross section defined by a 4% thick parabolic–arc aerofoil. The finite–element model, used to calculate the mode shapes for the modal structural model in the CFD formulation, follows the description given in [38]. Two cases are discussed, i.e. the clean wing and wing/store configurations, each retaining the four modes with the lowest frequencies (excluding in–plane modes) for the aeroelastic simulations. The frequencies as well as the mode shapes mapped to the CFD surface mesh for the wing/store configuration are shown in Fig. 1. Here, a relatively large value of two is chosen for the modal amplitudes for illustration purposes. A computational mesh with 200 thousand control volumes is used for the current Euler simulations while the store aerodynamics are not modelled.

Figure 2 gives one representative element of the Schur interaction matrix (excluding the bifurcation parameter) for the wing/store configuration showing real and imaginary parts individually. The black dots

in the figure indicate sample locations while the coloured surfaces represent the kriging predictions used for the stability analysis. Herein, the reconstruction is based on 40 samples covering a Mach number range between 0.7 and 0.95 and a dimensionless frequency range between 0.05 and 0.35. The sample frequencies were chosen according to the normal mode frequencies of the first two modes, thus not covering the third and fourth mode. The consequences of this are presented below. In the subsonic region, only small changes can be found in the response surfaces with respect to the input dimensions of response frequency and freestream Mach number, while there are significant variations in the transonic range, particularly with respect to the Mach number. Thus, the response surfaces show a similar behaviour as in the aerofoil study [24]. For freestream Mach numbers just below 0.9, marking the onset of the transonic range with distinct shock waves, the applied interpolation technique exhibits some minor difficulties predicting a wave–like oscillation in the interaction elements. This artefact is due to the (physically meaningful) strong changes in the response surfaces between Mach numbers of 0.9 and 0.95.

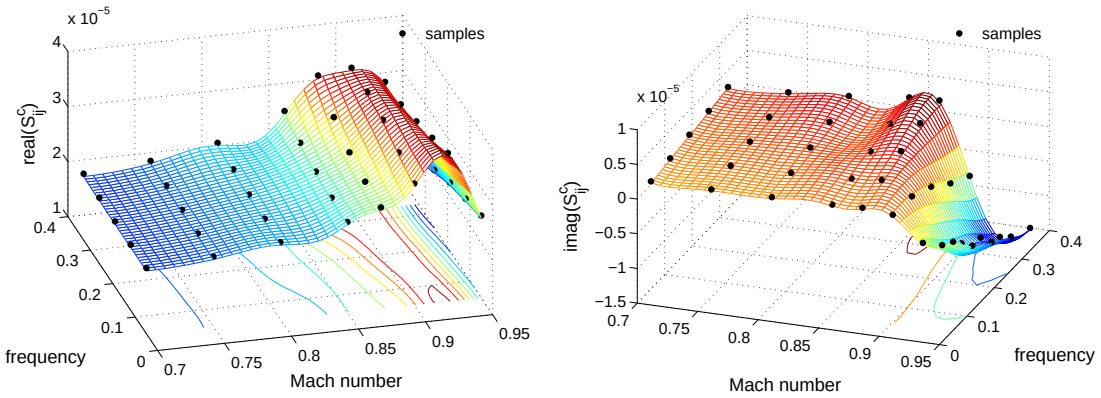

(a) real part (b) imaginary part

Figure 2. Extracted and interpolated element $S^c_{6,1}$ of Schur interaction matrix for Goland wing/store configuration using Euler flow model and first frequency domain approach for sample extraction.

Interestingly, for the flutter analysis using MSC.Nastran the aerodynamic influence coefficient matrix is evaluated at a limited number of points in the parameter space defined by the reduced frequency and Mach number. This is necessary as this evaluation significantly contributes to the computational cost. Then, an interpolation is applied to find the values between these discrete points [39]. Thus, the approach taken in this study is similar with two important differences. First, nonlinear CFD–based aerodynamic modelling is applied. Secondly, the parameter space in the current approach can easily be extended to include more parameter dependencies. Recall that the steady state solution, and consequently the interaction matrix, can depend on a large number of parameters. At this point of the current study only the dependence on the response frequency and freestream Mach number is considered, while later on for the MDO wing case the input parameter space will be extended.

The instability boundaries for the clean wing and wing/store configurations are presented in Fig. 3. Here, the boundaries are shown for the two types of matched simulations. The results for the instability onset with increasing velocity at fixed sea level conditions are compared with the numerical predictions in [38]. The results using the approximation approach are included. Importantly, the kriging approach gives excellent agreement with the full order predictions based on the series method. The simulation results using the quasi–Newton approach are not shown herein as they were found to be indistinguishable.

In Fig. 3(a) the clean wing configuration develops a clear transonic dip with a minimum critical velocity of about 110 m/s. Similarly, a somewhat flatter transonic dip is obtained for the wing/store configuration with a minimum velocity of about 180 m/s (stabilising the system). The basic features of the instability boundary, as discussed in [38], are found. At a freestream Mach number of about 0.9 the boundaries rapidly increase in both cases which is related to the formation of a strong shock wave. For the wing/store case, it is followed by a bucket of shock induced limit–cycle oscillation (LCO) at about Mach 0.92. Here, the dominant aeroelastic response changes from the (until then) first bending mode to the first torsion mode, which was confirmed in the present study through the critical eigenvalues. Note that the peak before the bucket of LCO is characterised by the third mode [38]. The results of time–accurate simulations, included in the figure at

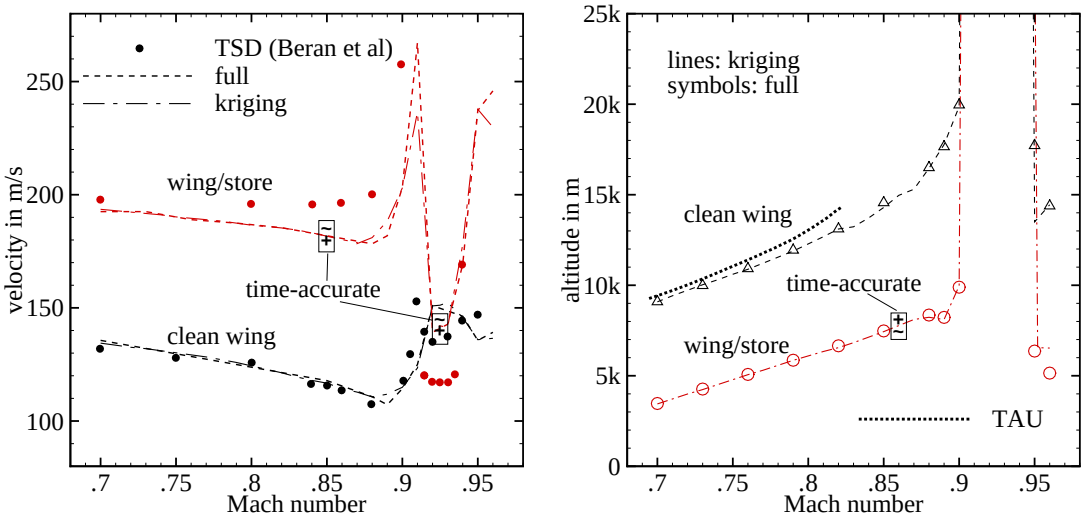

(a) Critical velocity at sea level conditions

(b) Critical altitude

Figure 3. Instability boundaries of Goland wing for matched simulations showing critical values of velocity and altitude compared with numerical results (where available) in [38]; TSD – transonic small disturbance.

two freestream Mach numbers, support the eigenvalue–based predictions with the plus (tilde) sign indicating a stable (unstable) response. In contrast to the lower Mach number at 0.85, the response signals of the generalised coordinates describe an instability strongly dominated by the second mode at Mach 0.925. The reasons for the discrepancy in the results with the transonic small disturbance (TSD) prediction from [38], particularly for the wing/store case, are not discussed further though as the most important target in this study, i.e. the agreement between the full order and approximation models, is achieved.

Similarly in Fig. 3(b), showing the instability boundaries with respect to altitude changes, the wing/store configuration gives a more benign response allowing flight operations at lower altitudes compared with the clean wing. Between freestream Mach numbers of 0.91 and 0.94 the aeroelastic system is unstable (dominated by the second mode) right from the start of the considered altitude range at 30 km. As above, the agreement between the full order results and the kriging approach is excellent. Also, the time–accurate results match the eigenvalue–based predictions. Figure 3(b) includes an additional set of results, denoted "TAU", which is taken from a preliminary study aimed at combining the Schur complement eigenvalue method, using the approach based on sampling and reconstruction, with the DLR TAU code [40].

Figure 4 shows the tracing of the four aeroelastic modes with respect to altitude changes and compares the different predictions. The full order predictions were obtained by applying the series method with a second order expansion. The agreement in both the mode tracing and the onset of the instability should be considered as excellent. The results show a classical binary instability mechanism with an instability occurring alongside the interaction of two aeroelastic modes involving the first bending and first torsion mode. In addition, the wing/store case gives a second instability at lower altitudes following the interaction of the third and fourth mode. There are two interesting aspects concerning the kriging formulation. First, as for the aerofoil case [24], the simplification of using an approximate Schur interaction matrix based on samples with zero damping is appropriate. The modes can be traced accurately even away from the imaginary axis (where the approximation is exact within the limits of the interpolation algorithm) suggesting that the variation of the structural part, $S^s(\lambda)$, with respect to the eigenvalue's real part is more dominant compared with the variation of the interaction term $S^c(\omega)$. Secondly, it must be remarked that the samples, used in this study for the reconstruction of the response surfaces, cover only the frequency range of the first and second wind–off structural modes up to a dimensionless frequency of 0.35. Thus, the kriging model extrapolates to deal with the two higher frequency modes while doing a good job. This also suggests that the influence of the interaction term on the structural eigenvalue problem for the higher frequency modes is relatively small. The sensitivity of the modes with respect to changes in the components of the interaction matrix will be addressed in the discussion of the MDO wing case.

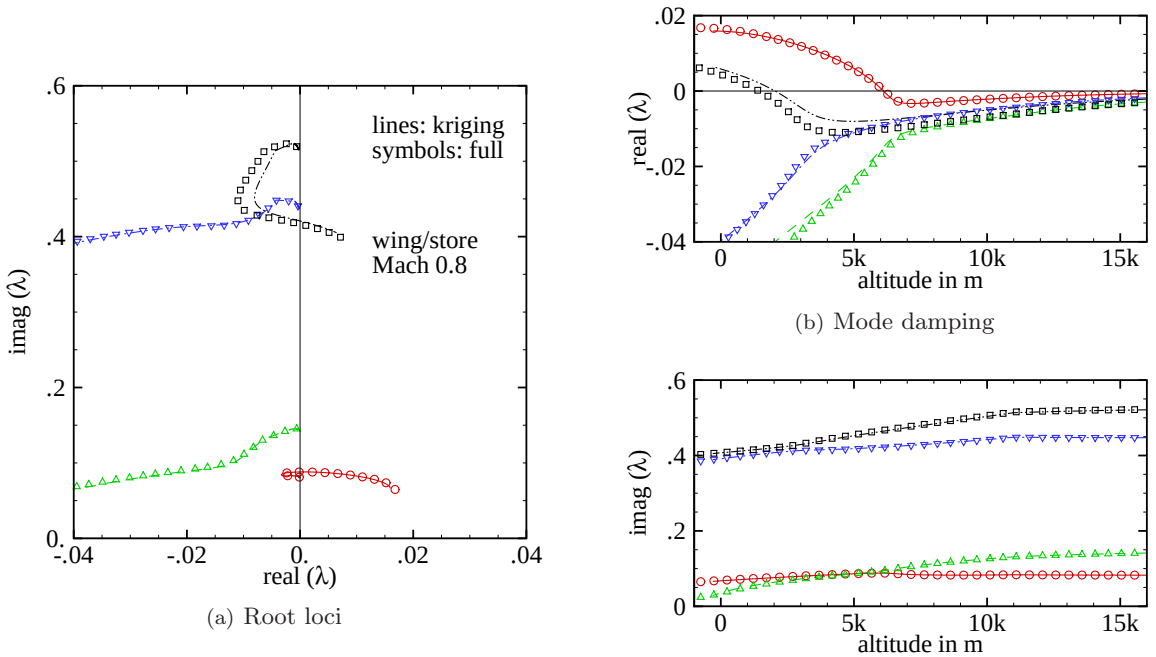

(a) Root loci

(b) Mode damping

(c) Mode frequency

Figure 4. Mode tracing at Mach 0.8 with respect to altitude for Goland wing/store configuration; eigenvalues given in dimensionless form.

For the reconstruction of the response surfaces in Fig. 2, 40 samples are used corresponding to the cost of $40 \times 2n$ linear solves against the fluid system (using the first frequency domain extraction approach) once the steady state solution is available. In the following one linear solve is taken as an equivalent cost factor because the solutions of the large sparse linear systems incur most of the involved cost. These samples allow the stability analysis covering an entire range of freestream Mach numbers between 0.7 and 0.95. Using the series method with a first order expansion, the evaluation of the series factors (for all four normal modes) takes $n \times 4n$ linear solves per Mach number, while tracing the modes can then be done essentially without additional cost. Recall that the series factors are valid only in the vicinity of the chosen shift λ_0, i.e. the normal mode frequency. Thus, with the fifth Mach number the cost invested in constructing the kriging model pays off. Also, the reconstruction approach becomes more powerful with an increasing number of normal modes as every individual sample supports the analysis/tracing of all modes while the series factors are only valid close to the shift they have been evaluated for. Note that the second frequency domain approach to extract the samples incurs half the cost of the first approach while giving identical results.

Once the approximation model is established, the stability analysis can be done essentially without additional cost no matter how large the original CFD–based system becomes. The aim of using kriging to interpolate the elements of the interaction matrix is to reduce the number of calculations for a blind search stability analysis over the flight envelope, i.e. for a range of flow conditions, as will be seen in the following. However, for a single point analysis excluding aerostatic effects it seems to be more advantageous to use the series method as the kriging model requires a minimum number of samples.

B. MDO Wing – Nonsymmetric Case with Aerostatic Effects

To include the effects of aerostatic deformation, the approximate Schur complement matrix used for the stability analysis is written in a fashion similar to Eq. (5),

$$S = \widetilde{S}^s(\lambda, h_r, M_r) + \mu(h_r, M_r)\, \widehat{S}^c(\omega, h_r, M_r), \tag{6}$$

with the difference that the modified interaction term now depends on the altitude h_r. As a consequence, the sampling has to cover the altitude range of interest. This however is equivalent to the requirements of the exact (full order) eigenvalue solver. Using the series method, the factors have to be re–evaluated constantly

as the modes are traced with changing altitude. Here, the altitude change before re–evaluation depends on the demanded accuracy. As will be seen below, the reconstruction of the interaction term using interpolation becomes very attractive concerning the cost.

The multidisciplinary optimisation (MDO) wing is a highly flexible, commerical transport wing designed to operate in the transonic range. It has a span of 36 m and a thick supercritical section. The nonsymmetric section makes the steady state solution dependent on the altitude, which is attractive for the current discussion. A computational mesh with 65 thousand control volumes is used for the current Euler simulations. The finite–element model is given by a wing box along the central portion of the wing [21]. For the aeroelastic stability analysis a total number of eight normal modes is considered with the mode shapes, mapped to the CFD surface grid, and the normal mode frequencies given in Fig. 5. This case is chosen to demonstrate the applicability of the kriging interpolation for the sampling and reconstruction approach to a higher number of normal modes and independent parameter dimensions. Due to the theoretical origins of the MDO wing, experimental data are not available [41].

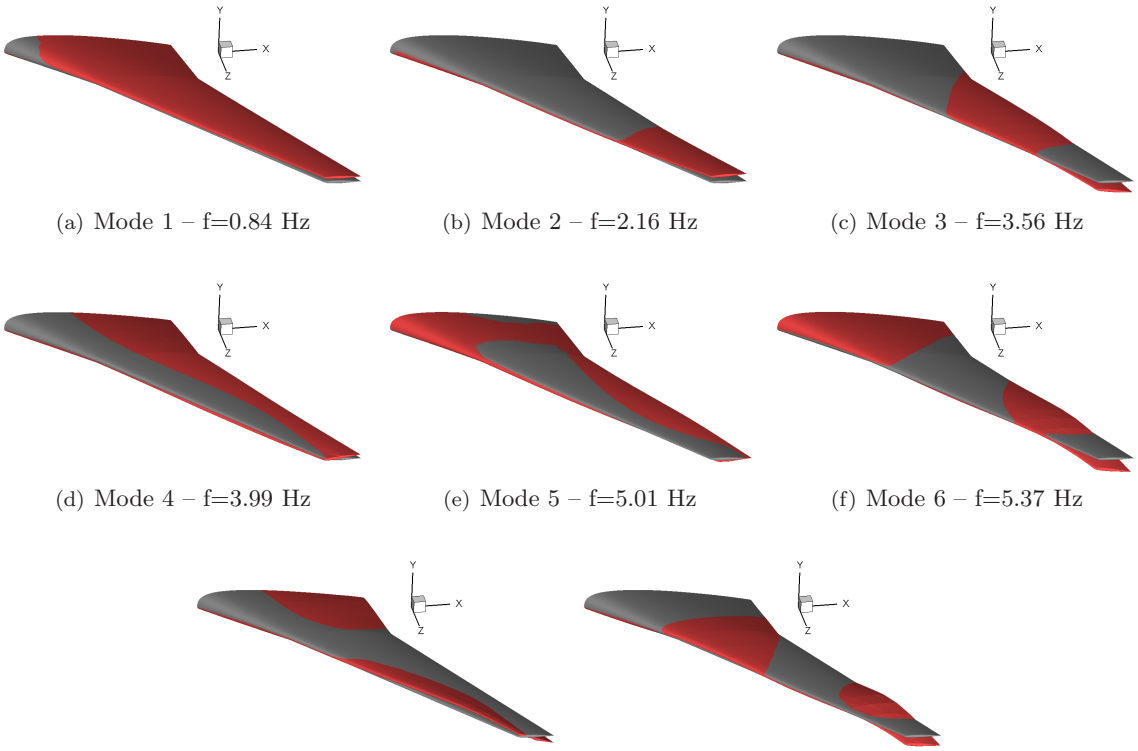

(a) Mode 1 – f=0.84 Hz (b) Mode 2 – f=2.16 Hz (c) Mode 3 – f=3.56 Hz

(d) Mode 4 – f=3.99 Hz (e) Mode 5 – f=5.01 Hz (f) Mode 6 – f=5.37 Hz

(g) Mode 7 – f=6.57 Hz (h) Mode 8 – f=7.30 Hz

Figure 5. Mode shapes of MDO wing configuration.

The influence of the aerostatic deformation on the steady state solution with varying altitude is presented in Fig. 6 and compared with the results of a rigid wing simulation. The flow is simulated at a fixed transonic freestream Mach number of 0.85 and zero degrees angle of attack. It can be seen that a decreasing altitude, corresponding to an increase in the dynamic pressure, causes the wing to bend up and to twist the nose down slightly at the wing tip. The aerostatic deformation results in a weakened shock wave, present on the upper surface of the wing. Note the differences in the colour legends for the (dimensionless) pressure between the rigid and deformed wing cases.

Figure 7(a) gives one representative element of the Schur interaction matrix in the frequency/altitude parameter space with a freestream Mach number of 0.85 and zero degrees angle of attack corresponding to the conditions shown in Fig. 6. The reconstruction is based on 32 samples covering dimensionless frequencies of up to 2.2 (according to the structural frequencies) and an altitude range of up to 15 km for normal operational flight conditions. In the figure, the magnitude of the modified interaction term should not be misinterpreted. The results are plotted for the bifurcation parameter set to unity. Multiplication with the actual value of this parameter introduces a factor of the order 10^6 in the region of the instability. As the

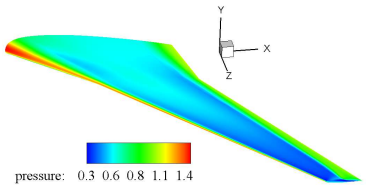

(a) Pressure distribution: rigid wing

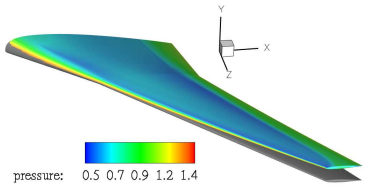

(b) Pressure distribution: flexible wing at 15 km

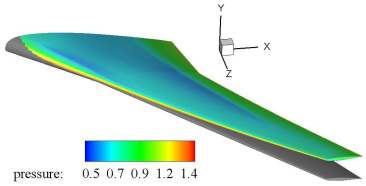

(c) Pressure distribution: flexible wing at 9 km

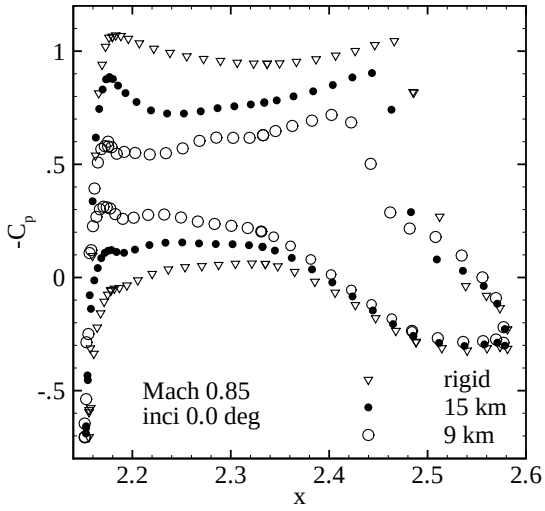

(d) Pressure coefficient at $z = 1.3$

Figure 6. Effect of aerostatic deformation on surface pressure distribution at Mach 0.85 and zero degrees angle of attack for MDO wing.

shape of the shown response surface is not particularly intuitive, in contrast to a Mach number dependence, an attempt is not made to interpret it further. The kriging approximation of the interaction matrix is then applied to the aeroelastic stability analysis.

The results of such a stability analysis including aerostatic effects are presented in Fig. 8. The figure gives an accurate tracing of all considered modes compared with the full order results using the series method. Here, the series factors (just as the steady states) were re–evaluated at each new altitude for reasons of accuracy for the comparisons with an applied decrement of 500 m. The first mode goes unstable at an altitude of about 4.5 km, closely followed by the second mode crossing the imaginary axis at about 3.8 km. The differences in the frequency at lower altitudes for the fourth mode are due to the strongly damped character of this mode. The assumption of a simple harmonic aerodynamic response, i.e. $S^c(\omega)$ instead of $S^c(\lambda)$, does not hold in this case. However, this behaviour is irrelevant for the stability prediction.

For the sake of completeness, the influence of the small second term $\mu\, C_2$ in the structural part of Eq. (4) is considered. Therefore, a second kriging model was formed based on full order samples which are routinely evaluated alongside the samples of the interaction term. These samples allow the reconstruction of the corresponding response surfaces depending on the altitude. This dependence is then included in the stability analysis. However, these "improved" predictions are within plotting accuracy compared with the results given in Fig. 8, and hence they are neither shown nor further discussed.

The issue of cost is analysed for the case with aerostatic deflection. For the reconstruction of the response surface in Fig. 7(a) using the first frequency domain approach, 32 samples are used which is equivalent to the cost of $32 \times 2n$ linear solves plus the evaluation of the steady state at each altitude. Evaluating one steady state corresponds to solving approximately $2n$ linear systems in this case. The achieved resolution of the reconstructed response surfaces is sufficient to trace the eight normal modes accurately compared with the full order results. Using the series approach in the full order formulation on the other hand, the series factors (just as the steady states) have to be recalculated several times as the altitude is decreased due to

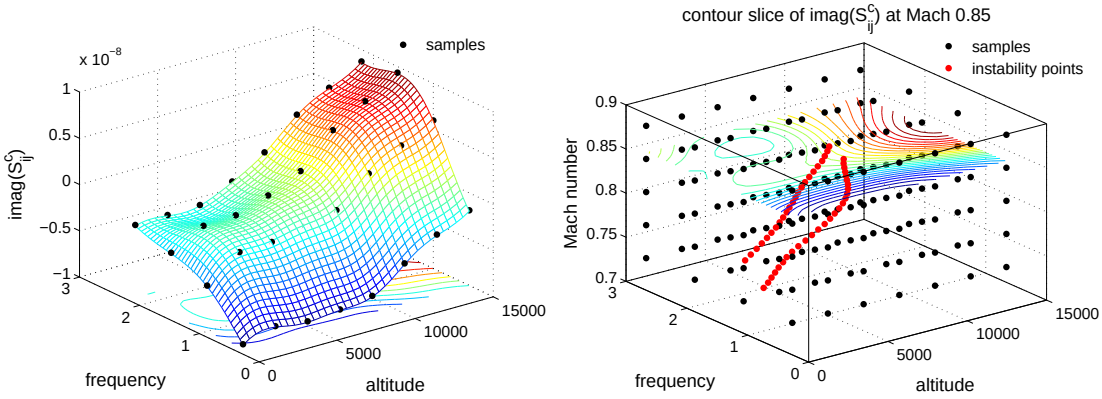

(a) two dimensional grid sampling

(b) three dimensional grid sampling

Figure 7. Extracted and interpolated element imag($S^c_{10,1}$) of Schur interaction matrix for MDO wing configuration showing (a) two dimensional grid sampling depending on altitude and dimensionless frequency at Mach 0.85 and zero degrees angle of attack and (b) three dimensional grid sampling at zero degrees angle of attack including trace of instabilities.

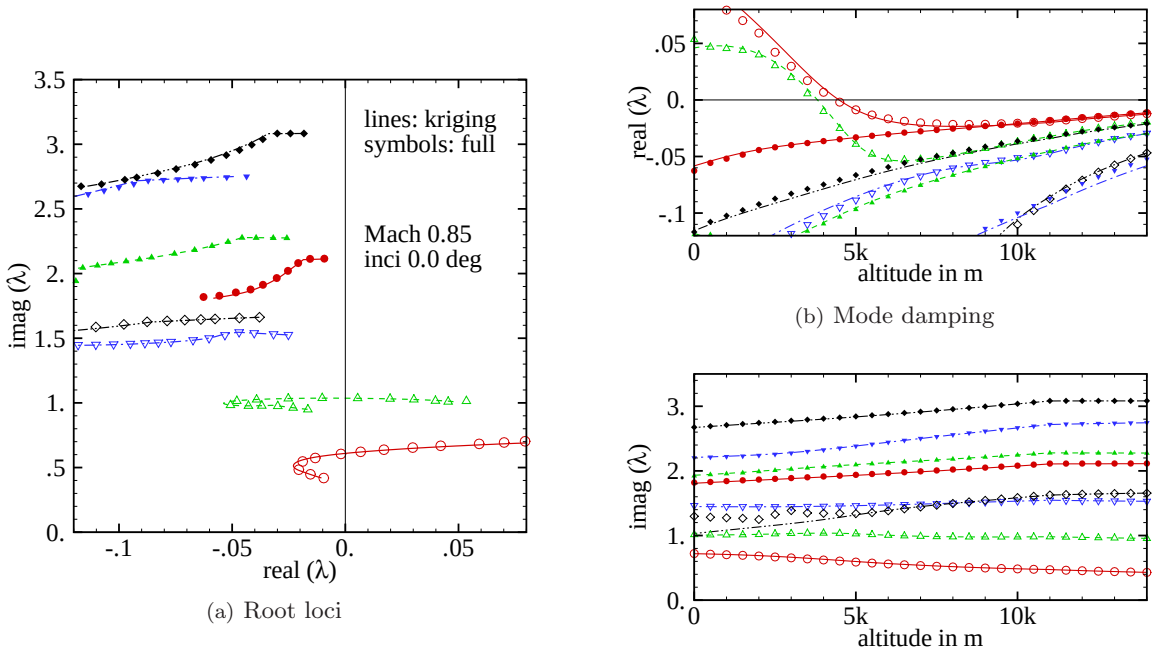

(a) Root loci

(b) Mode damping

(c) Mode frequency

Figure 8. Mode tracing for MDO wing configuration with respect to altitude at Mach 0.85 and zero degrees angle of attack; eigenvalues in dimensionless form.

the included aerostatic deformation. One evaluation of the factors (for an expansion up to first order) for all eight modes takes $n \times 4n$ linear solves. Thus, the cost of forming the approximation model pays off after only the second re–evaluation of the series factors (or, when using the second extraction approach, after the first re–evaluation). Note, for the demonstration shown in Fig. 8, the series factors were calculated at each new altitude (which makes it quasi–Newton) for reasons of accuracy.

The challenge for the kriging approach as discussed up to this point is not the inclusion of aerostatic effects at fixed freestream Mach number but the search for aeroelastic instability over the flight envelope, i.e. a range of freestream Mach numbers. Figure 7(b) shows the distribution of 140 samples for the reconstruction

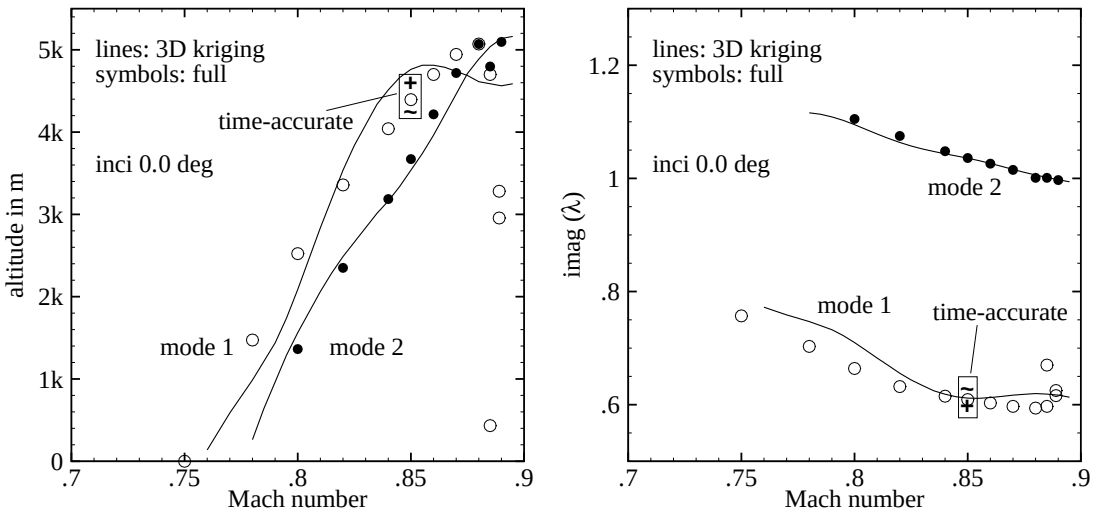

(a) Critical altitude (b) Critical frequency

Figure 9. Stability results for MDO wing configuration using three dimensional grid sampling showing critical values of altitude and dimensionless frequency.

of the interaction matrix depending on altitude, frequency and Mach number. The contour slice for one representative interaction element at the freestream Mach number of 0.85 clearly resembles the response surface given in Fig. 7(a). Also, the traces of the first and second mode instabilities are included in the figure to illustrate the important region of the parameter space.

This stability limit over a range of freestream Mach numbers between 0.7 and 0.9 is presented in Fig. 9 as critical values of altitude and dimensionless frequency. For freestream Mach numbers below 0.75, the configuration only encounters aeroelastic instability below sea level while at common cruise conditions the critical region starts at about 5 km. In addition, the first mode exhibits a second bifurcation at the highest Mach numbers, which is below the second mode instability and therefore not of immediate interest. As can be seen in the figure, a reasonable agreement between the kriging and full order results is achieved. In the previous aerofoil study [24] it was found that changes in the interaction matrix with respect to the freestream Mach number (due to the formation of shock waves) are often more significant compared with frequency changes which would require more samples in the dimension of the Mach number to resolve the changes. In the current case for the MDO wing configuration, samples are calculated at five Mach numbers between 0.7 and 0.9 posing a challenge to the interpolation as this parameter dimension might be undersampled.

To support the eigenvalue predictions, time–accurate simulations were done at Mach 0.85 with the plus (tilde) sign in the figure indicating a stable (unstable) response. The agreement is excellent and the time–accurate responses are dominated by the first unstable mode. The time–accurate simulations run with a dimensionless time step of 0.05 for temporal accuracy given 210 steps per cycle of motion for a dimensionless response frequency of about 0.6. Then, one motion cycle corresponds to two steady state simulations. Close to the instability point however the time–accurate transient covers several motion cycles, and several time domain runs are required per Mach number to bracket the instability point.

Assume that four Mach numbers along a flight envelope are to be investigated while considering aerostatic effects. Generously, for an altitude search range of 15 km the series factors are re–evaluated only four times creating an equivalent cost of $4 \times 4 \times n \times 4n$ linear solves for the eight normal modes. Thus, the 140 samples, requiring $140 \times 2n$ linear solves, generate about half the cost while giving competitive results. Recall the further cost reduction using the second approach. In the next section, the powerful approach of coordinated sampling shows how the prediction is improved with less samples.

Importantly, the stability limit for the rigid MDO wing without the effects of aerostatic deformation is presented in Fig. 10. The results demonstrate the importance of including the effects of aerostatic deformation in the transonic aeroelastic stability analysis. The stability characteristics are significantly changed as can be seen in the figure. The typical transonic dip, related to the first bending mode

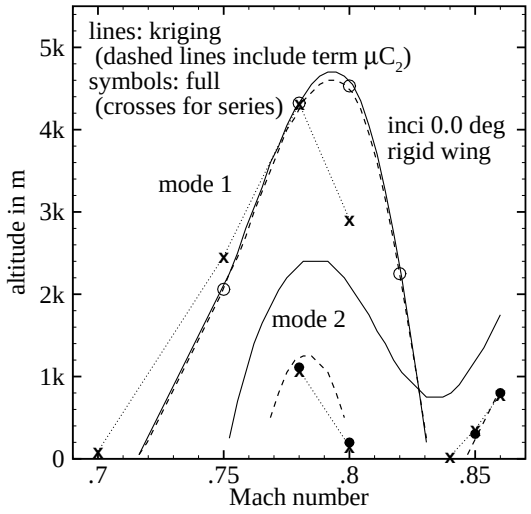

Figure 10. Stability analysis for rigid MDO wing configuration at zero degrees angle of attack showing critical values of altitude comparing full order and kriging approximation results.

going unstable, is formed and shifted to lower Mach numbers compared with the results including aerostatic deformation in Fig. 9. This should be attributed to the formation of the transonic shock waves. The shock strengths are reduced by the aerostatic deformation compared with the rigid wing case as can be seen in the pressure distribution given in Fig. 6.

Several observations concerning the presented eigenvalue–based stability analysis can be given. First, note the differences in the results from the exact eigenvalue solver using the series method (with a second order series expansion) and the quasi–Newton approach. Here, distinct differences are found, particularly for the instability associated with the first bending mode. This demonstrates the limits of the series expansion in some situations for larger variations in the response frequency (relative to a chosen shift). Thus, the series approach is very useful and efficient but the robustness and accuracy should always be considered. Secondly, the agreement of the kriging–based simulations with the quasi–Newton results is excellent as expected since the kriging approximation is based on exact numerical samples. Thirdly, a second kriging simulation is shown. These additional results consider the effect of the second term μC_2 in the structural part of the Schur complement matrix in Eq. (4) on the stability analysis. The influence on the first mode is negligible while, surprisingly, the second mode instability is significantly changed correcting the prediction towards the full order reference results. In this case, the variation of the force vector with respect to the structural unknowns cannot be neglected.

Now it is assumed that the kriging model does a good job to precisely reconstruct the response surfaces of the interaction matrix elements giving an exact representation of the physics from the full order model. Further, it is assumed that the uncertainty in the aerodynamic modelling is reflected in the response surfaces. Then, the cheap approximation model can be exploited to analyse the sensitivity of the eigenvalue problem on the elements of the interaction matrix. Figure 11 shows the sensitivity of the mode tracing with respect to a 20% variation randomly distributed over the nonzero elements of the interaction matrix. In the figure the sensitivity is expressed by one standard deviation about the mean. Theoretically, it is possible to find the sensitivity of the system response with respect to each element individually due to the low cost of the approximation model. However, this is not attempted at this point for two reasons. First, it should always be possible to evaluate one complete sample (i.e. one complete interaction matrix). Secondly, it seems to be more important to place complete samples in the right spot in the parameter space, the information of which can be derived from the sensitivity of the traces. In this case the results demonstrate that the relatively large variation does not give any tendency of the six higher frequency modes to go unstable while the first and second mode give rise to some uncertainty about the onset of the instability. The predicted frequencies are basically unaffected. In addition, this information would allow the estimation of the importance of using higher fidelity (more expensive) aerodynamic models, and, if considered to be important, the relevant locations to place the better samples.

IV. Coordinated Sampling and Model Updating

The main computational task for the Schur complement eigenvalue method is to approximate the interaction matrix to describe the fluid response accurately. The goal of the research is to enable aeroelastic instability searches over the flight envelope, and in this section it is achieved by introducing searches for the approximation of the interaction matrix. The stability analysis is demonstrated using aerodynamic models of variable fidelity.

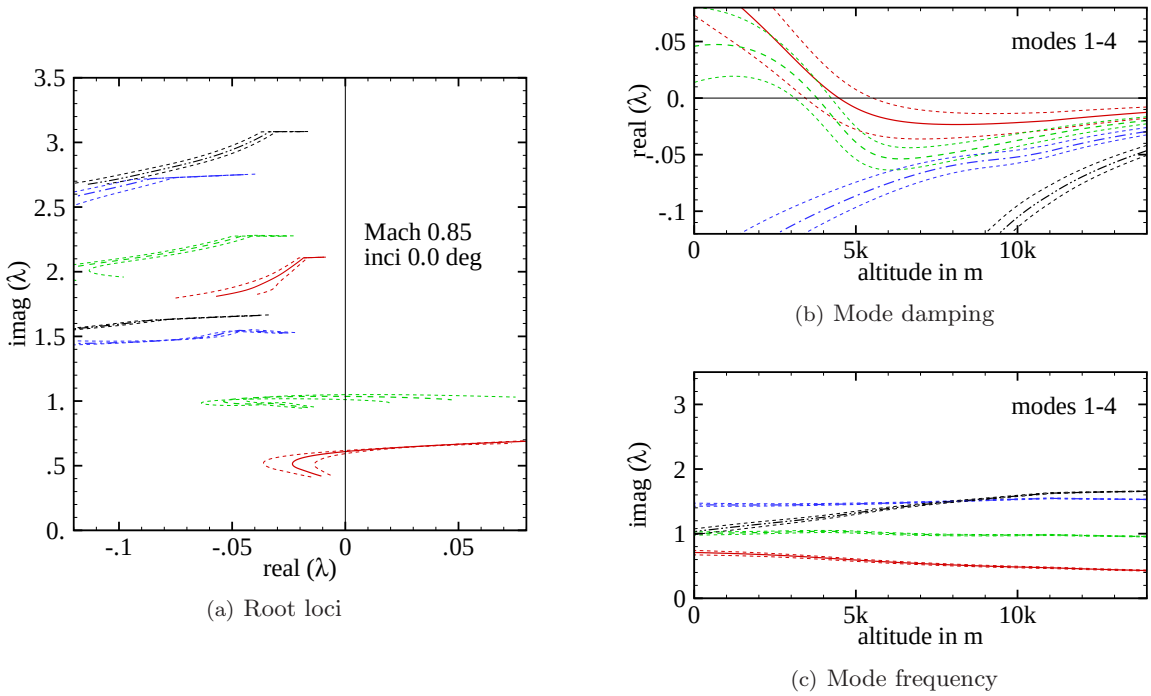

(a) Root loci

(b) Mode damping

(c) Mode frequency

Figure 11. Sensitivity of mode tracing for MDO wing configuration at Mach 0.85 and zero degrees angle of attack showing one standard deviation due to 20% variation in elements of interaction matrix.

A. Coordinated Sampling

MDO Wing Configuration

The risk–based sampling approach, introduced in the previous aerofoil study [24], is now examined for the MDO wing configuration using the modal structural model and including the effects of aerostatic deformation. First, the possible reduction of required samples at fixed Mach number is discussed. Then, additional input parameter dimensions are added to demonstrate the generality of the approach.

In Figs. 12 and 13, the risk–based sampling is presented for the MDO wing case at Mach 0.85 and zero degrees angle of attack, corresponding to the above discussion. The effects of aerostatic deformation are fully accounted for. The sampling proceeds in a fashion similar to the aerofoil cases [24]. First, a search space is defined by the corner samples covering the altitude range of interest and the frequency range according to the structural frequencies giving 2^m initial samples for the $m = 2$ independent parameter dimensions. Then, the eight modes are traced with varying altitude under matched conditions using the cheap approximation model based on the current set of samples, and the instability points are detected. Having more than one bifurcation point, the location with the highest standard error in the kriging prediction gives the new sample location, or alternatively the most critical condition, i.e. the highest altitude, can be chosen. Alternative sampling criteria, for example a positive gradient in the eigenvalue's real part with respect to the altitude, are possible. Such a risk–based sampling guarantees that samples are always placed at locations where they support the prediction most in terms of risk, i.e. at previously evaluated instability points, and improvement, i.e. at the location of the maximum error in the kriging model. Changes in the instability prediction between two consecutive iterations define a possible convergence criterion.

The sampling converges rapidly as can be seen in Fig. 12(a) showing one representative element of the interaction matrix, the sample distribution and the instability points for the first and second mode projected onto the response surface. After the third iteration, starting from the four samples of the initial search space, a new sample location matches the predicted instability points very closely. Continuing to iterate is neither necessary nor useful as the correlation matrix of the kriging model becomes increasingly ill–conditioned for sample points near previously sampled points [36]. Thus, the seven sufficient risk–based samples mean a cost reduction by a factor of about five compared with the grid sampling shown in Fig. 7(a).

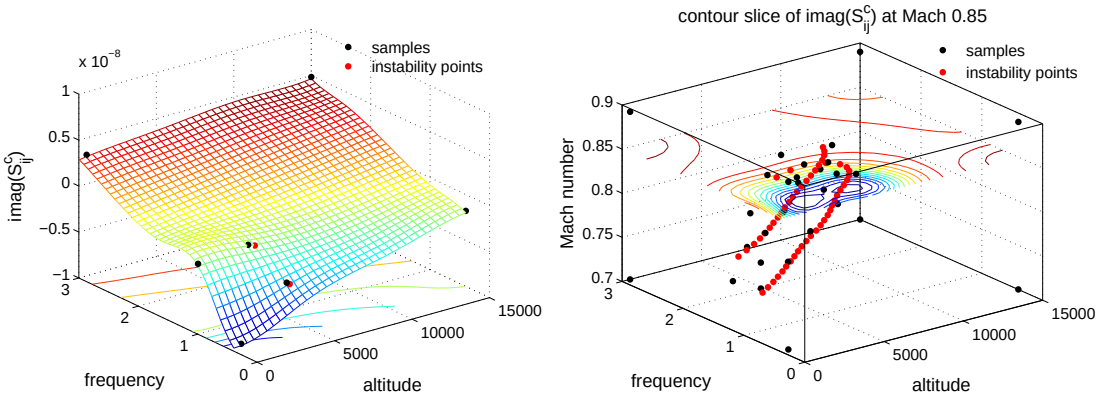

(a) Two dimensional search space

(b) Three dimensional search space

Figure 12. Two and three dimensional risk–based sampling for MDO wing configuration showing approximated element imag($S^c_{10,1}$) of Schur interaction matrix including projected instability points.

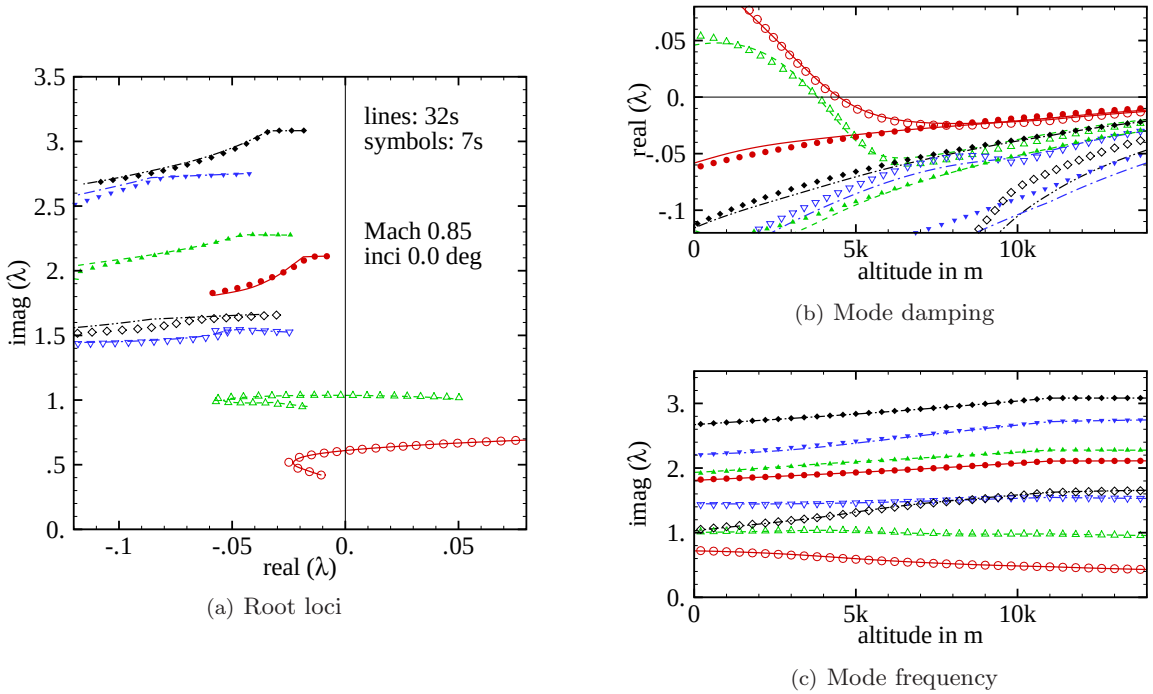

(a) Root loci

(b) Mode damping

(c) Mode frequency

Figure 13. Risk–based sampling technique showing mode tracing for MDO wing configuration with respect to altitude at Mach 0.85 and zero degrees angle of attack; eigenvalues given in dimensionless form.

Figure 13 compares the mode tracing using the kriging models based on 32 samples from the uniform grid sampling in the previous section and the seven samples from the current risk–based sampling. Interestingly, the agreement is excellent also for the higher frequency modes throughout both the altitude and frequency range, even though large parts of the parameter space are essentially uncovered by samples. Consequently, accurate response surfaces are not evaluated globally. There are two points to this observation. First, at high altitudes the influence of the interaction term is relatively small compared with the structural part as the density, defining the bifurcation parameter, is low. Secondly, the higher frequency modes are very insensitive to changes in the interaction matrix elements and the initial search space already gives a good enough approximation. Looking at the equations of the structural model and the Schur complement matrix in Section II, it is clear that the higher the normal mode frequencies, the more dominant the structural part

S^s on the eigenvalue problem becomes. A sensitivity study for the interaction matrix elements, as described in the previous section, was done to confirm the latter point and to reduce the risk of missing an additional (possibly more critical) bifurcation point for the higher frequency modes. In this case neither of the higher frequency modes showed any tendency to go unstable, while the uncertainty in the first two modes was similar to the results in Fig. 11.

In the previous section the prediction of transonic aeroelastic instability over a range of freestream Mach numbers was demonstrated using three dimensional uniform grid sampling. The risk–based sampling for higher parameter dimensions proceeds in the same fashion. First, the initial (multidimensional) search space is defined with the corner samples. Then, the instability points for the range of freestream Mach numbers and a chosen angle of attack are evaluated with the kriging model based on the current set of samples. The predicted instability point maximising the corresponding kriging error of the approximated interaction term defines the new sample location. Iteration converges the prediction. The risk–based sampling is herein demonstrated for three and four dimensional parameter search spaces with the parameters influencing the aerodynamic model. The initial sets of samples to define the search space are as follows. The third dimension for the freestream Mach number covers a range between 0.7 and 0.89. The fourth dimension covers angles of attack between minus and plus half a degree. For the current study, the chosen angle of attack to predict the stability limit is then set to zero degrees according to the preceding discussion.

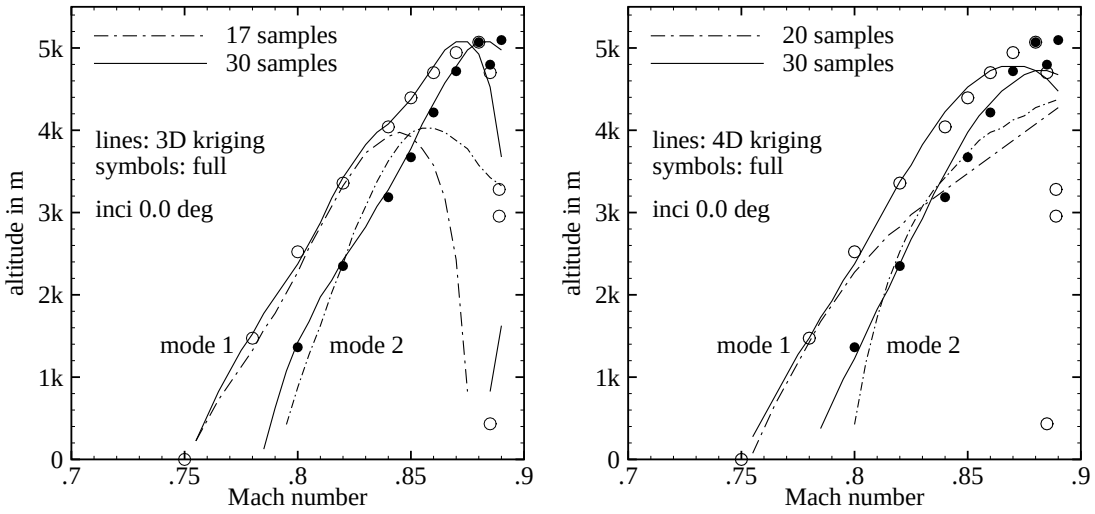

(a) Three dimensional risk–based sampling

(b) Four dimensional risk–based sampling

Figure 14. Instability boundary from three and four dimensional risk–based sampling for MDO wing configuration showing critical values of altitude.

Results are presented in Figs. 12(b) and 14. An impression of both the sample distribution and the response surface at Mach 0.85 is given in Fig. 12(b). The instability boundaries as critical values of altitude and dimensionless frequency for the three and four dimensional search spaces are given in Fig. 14. The three dimensional risk–based sampling, requiring 30 samples for accurate results, gives excellent agreement with the full order predictions. The 30 samples correspond to a cost reduction by a factor of about five compared with the three dimensional grid sampling. Also the second bifurcation of the first mode is found. The four dimensional sampling is less accurate at the higher freestream Mach numbers requiring more samples to converge. Note that for the current results the sampling criterion focuses on all instability points. Alternatively, it is possible to search only for the most critical condition which would be either the first or second mode in this case depending on the freestream Mach number. Adding the fourth dimension to the sampling problem demonstrates an interesting point about the approach. The approximation model can be updated for changes in the system parameters by adding additional samples that account for these changes, e.g. additional samples for different angles of attack. All the previously sampled points are kept to support the prediction as the approximation model grows gradually depending on the requirements. Thus, the re–use of samples is a major advantage of the kriging approach.

Open Source Fighter

A realistically sized aircraft model is considered next to demonstrate the presented approach for such cases. The idea was to establish a test case[b] with an aeroelastic behaviour representative of an aircraft, and thus the presented open source fighter, previously discussed in [22, 23], was built on data publically available for the F–16 aircraft. Available data for the wing geometry (dimensions and aerofoil section) together with published data from ground vibration and wind tunnel tests were used.

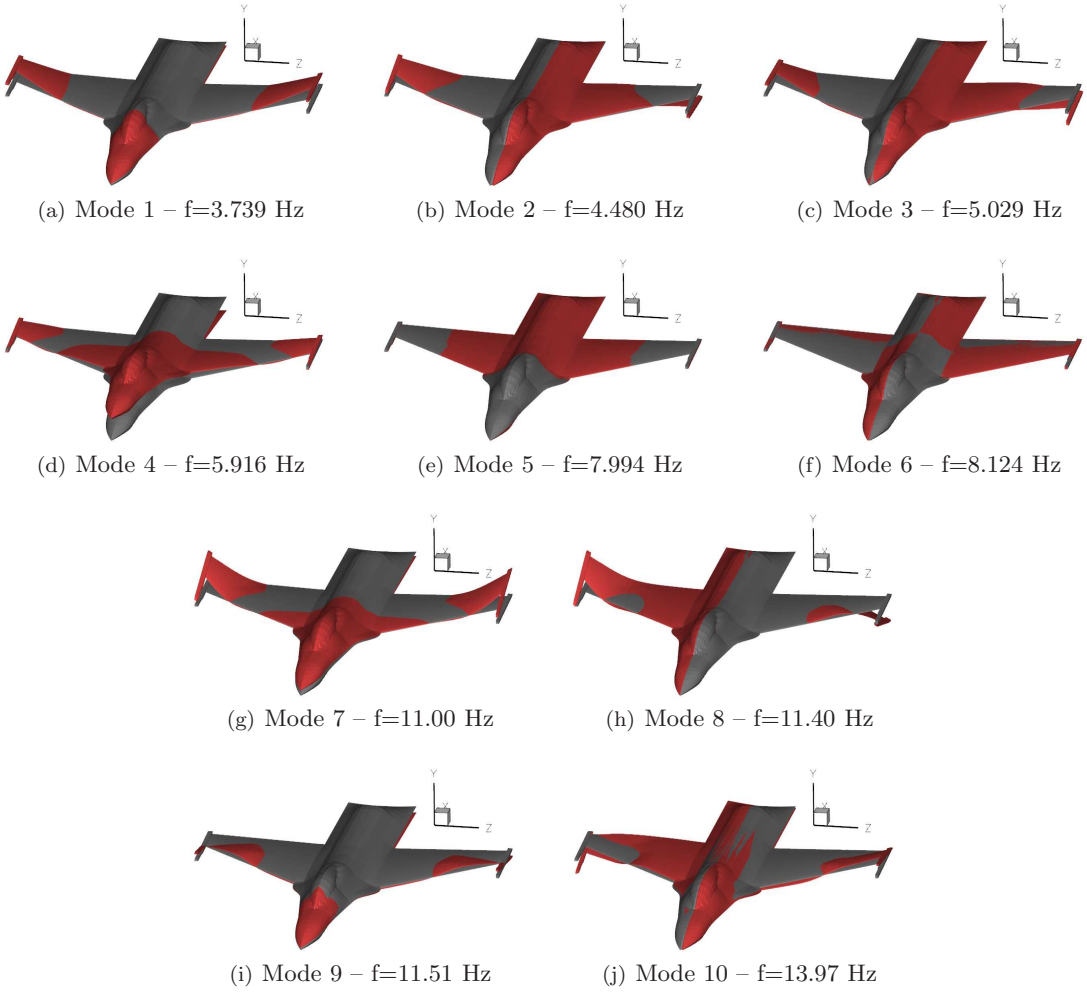

(a) Mode 1 – f=3.739 Hz (b) Mode 2 – f=4.480 Hz (c) Mode 3 – f=5.029 Hz

(d) Mode 4 – f=5.916 Hz (e) Mode 5 – f=7.994 Hz (f) Mode 6 – f=8.124 Hz

(g) Mode 7 – f=11.00 Hz (h) Mode 8 – f=11.40 Hz

(i) Mode 9 – f=11.51 Hz (j) Mode 10 – f=13.97 Hz

Figure 15. Mode shapes of open source fighter configuration.

The aerofoil section consists of a NACA 64A204 profile, with a wing root angle of −1.0 degree and a wing tip angle of −2.4 degrees. The twist was chosen by comparing with published surface pressures for the F–16 aircraft. The finite–element model of the configuration was built in MSC.Nastran based on the model proposed in [42]. The structural model consists of four parts including the fuselage, wing, pylon and stores. The fuselage, pylon and stores are considered to be effectively rigid. The mass properties of the pylon and stores are represented by lumped masses. The pylon is rigidly connected to the wing. The store is connected to the pylon by six spring elements (three translational and three rotational). The wing is modelled using shell elements and is divided into three regions including the root, pylon, and tip. In order to match the natural frequencies of the finite–element model to those found in ground vibration tests [43], the Young's modulus and density of each wing region are considered as updating parameters. Ten normal modes participating in the aeroelastic mechanism are retained for the current analysis. Figure 15 shows the mode shapes mapped to the CFD surface grid and the normal mode frequencies. For the current Euler simulations a relatively coarse grid with about 850 thousand control volumes is used.

[b]Files defining the model are available at http://cfd4aircraft.com/

Figure 16 shows the tracing of the ten normal modes with respect to changes in the altitude and compares the results from the full order simulation (using the series method) with the kriging approximation. The approximation model of the Schur interaction matrix is based on 40 samples uniformly distributed over the frequency/Mach number parameter space covering dimensionless frequencies of up to 1.0 and freestream Mach numbers between 0.7 and 0.9. The samples were extracted using the second frequency domain approach. The effects of aerostatic deformation are currently not considered, eliminating the dependence of the modified interaction term on the altitude as discussed for the Goland wing. An excellent agreement is found between the series and kriging results. At the chosen conditions the configuration goes unstable with the interaction of the second and third mode at an altitude of about 1450 m. This is followed by a second instability at about −4000 m due to the first and fourth mode interacting.

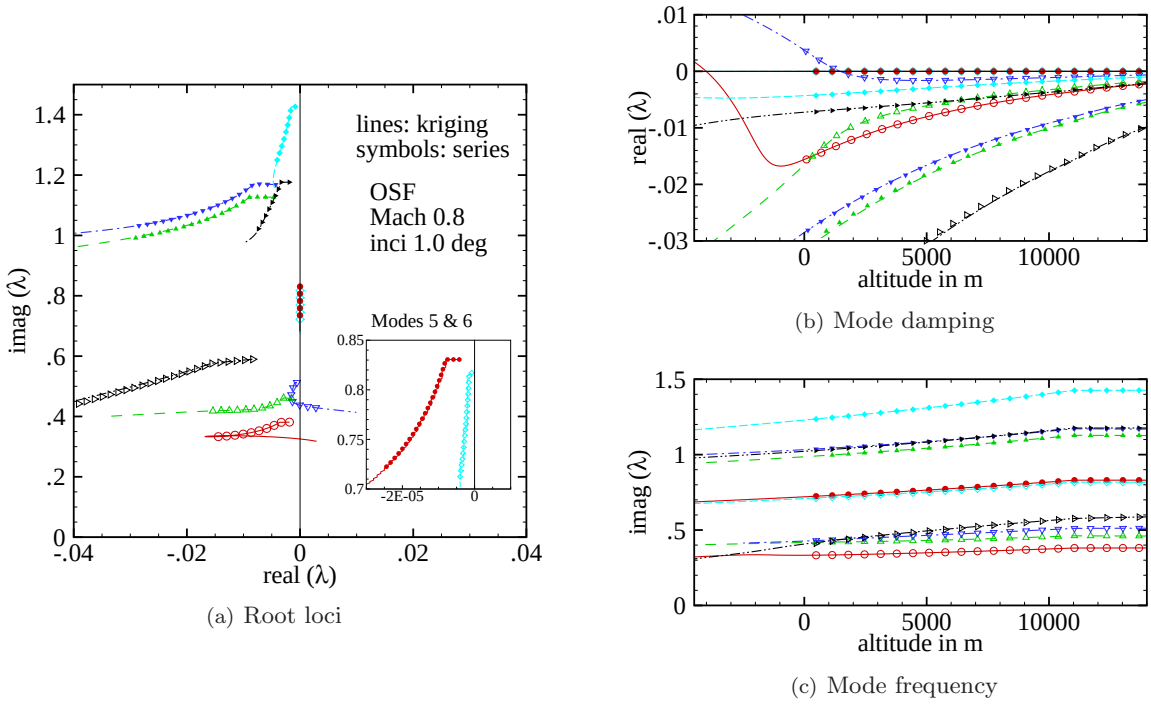

(a) Root loci

(b) Mode damping

(c) Mode frequency

Figure 16. Mode tracing with respect to altitude for open source fighter (OSF) configuration at Mach 0.8 and one degree angle of attack; eigenvalues given in dimensionless form.

Figure 17 gives the instability boundary for the considered range of freestream Mach numbers showing critical values of altitude and dimensionless frequency for the first and third mode instabilities. The results from the kriging approximation using both grid and risk–based sampling are compared. Following the agreement between the series and kriging predictions at Mach 0.8, additional Mach numbers have not been analysed for the current study using the full order approach. The instability behaviour is rather simple for the discussed conditions. Interestingly, using risk–based sampling the four initial samples to define the search space already give a very good approximation of the interaction matrix elements (not shown) to predict the instability boundary. Note that the search criterion for the analysis of the open source fighter only considers the most critical conditions, thus focussing the samples to predict the third mode instability. This is different to Fig. 14 where samples were chosen by the sampling criterion to predict all possible instability points precisely.

The discussion of cost is very interesting for the open source fighter retaining ten normal modes. For the approximation of the interaction matrix in this example using the grid sampling a total number of 40 samples was used. These samples correspond to $40 \times n$ linear solves for the second frequency domain extraction approach. This is about the same cost as using the series method (with a first order expansion) to evaluate the series factor for the ten relevant structural frequencies per steady state solution, i.e. $n \times 4n$ linear solves. The ten risk–based samples required to give an excellent prediction of the instability boundary in Fig. 17 result in a further cost reduction by a factor of four.

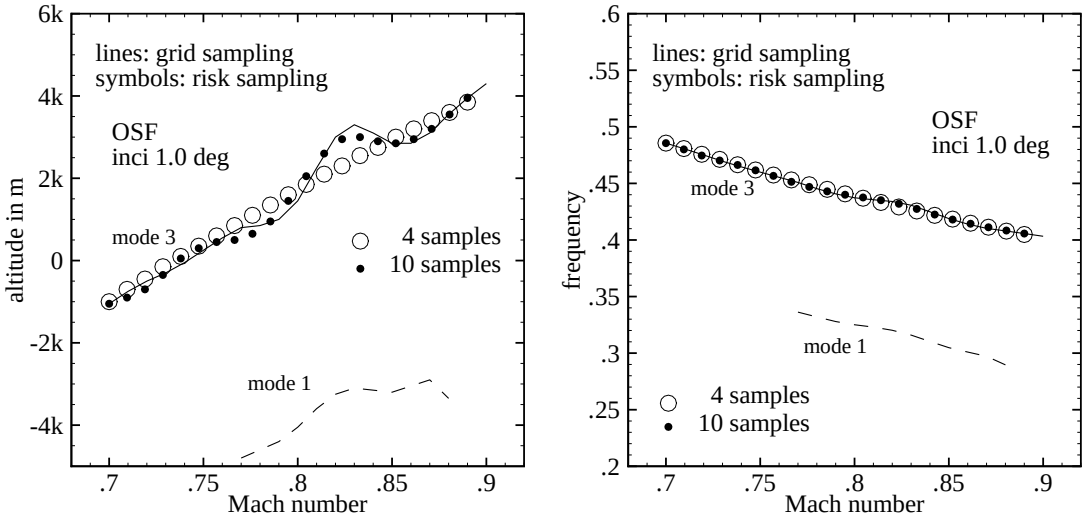

(a) Critical altitude

(b) Critical frequency

Figure 17. Instability boundary from kriging–based analysis using grid and risk–based sampling for open source fighter (OSF) configuration showing critical values of altitude and dimensionless frequency.

B. Model Updating – Goland Wing/Store Configuration

In [24] it was demonstrated for an aerofoil case how aerodynamic models of variable fidelity can be exploited to update a lower fidelity prediction with higher fidelity information. Three basic steps were shown to be useful. First, a few high fidelity samples of the interaction matrix were calculated based on the information provided by a lower fidelity stability analysis to avoid a blind search with the computationally expensive model. Secondly, the small set of high fidelity samples was augmented by the lower fidelity samples at the corners of the initial search space to support the construction of the high fidelity kriging model. This follows the observation of the risk–based sampling where the samples close to the aeroelastic instability are of most importance for accuracy. This is approximately satisfied by the high fidelity samples. Thirdly, the trend information of the response surfaces as provided by the lower fidelity prediction is used to support the high fidelity model assuming there is a correlation in the response surfaces for changing values of the system parameters. This correlation is found if the dominant flow physics are captured by the relevant aerodynamic models. The technique referred to as co–kriging was applied.

Next, the co–kriging approach is applied to the Goland wing/store configuration using the Euler and RANS equations from the model hierarchy. The Euler results follow the above discussion, while the RANS simulations are done using the two equation $k-\omega$ turbulence model and an H–type computational grid with about three million control volumes. The first wall normal grid spacing is 6×10^{-6} in dimensionless units. Also, a coarser level with about 350 thousand control volumes was extracted from the finer level grid maintaining a first grid spacing of 1.4×10^{-5}. The chord Reynolds number is specified to be 15 million following [38] and is not varied in this study strictly violating matched conditions according to the freestream Mach number and altitude. Representative surface pressure distributions for the Euler and RANS simulations are shown in Fig. 18(a) at a freestream Mach number of 0.9 and two locations in the spanwise direction close to the wing root and wing tip. A strong shock wave is formed near the wing root weakening towards the tip. The differences between the two flow models are relatively small as expected considering the high reference Reynolds number. The shock location moves marginally upstream in the RANS results while the characteristic inviscid overshoot at the bottom of the shock wave is corrected by the viscous effects.

The constant volume tetrahedron (CVT) transformation [30] is applied in the multiblock flow solver to transfer information, i.e. pressure forces and deflections, between the fluid and structural grids. It is a local intergrid transfer method which means that the grid locations at the boundaries of structural elements (defined by three structural grid points) are matched while the slope is not. One can imagine that linear extrapolation, which is required for the Goland wing behind the two thirds chord line, amplifies the effects of this slope difference causing a zigzag–like mapping at the trailing edge for fine fluid grids. The problems caused by extrapolation using CVT are also found for the Euler computational grids. However, as the Euler

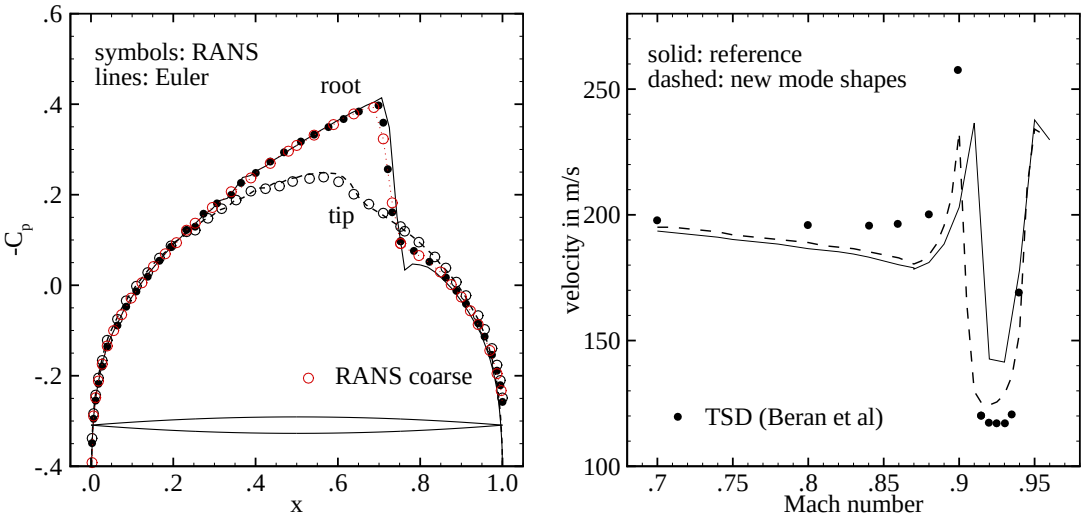

(a) M_r=0.9, α=0.0°, Re=15.0×10^6 (b) Critical velocity at sea level conditions

Figure 18. Surface pressure distribution for Goland wing comparing Euler and RANS flow models at two freestream Mach numbers and two spanwise locations, and instability boundary for Goland wing/store configuration showing critical values of velocity at sea level condition.

grid resolution is coarser compared with the RANS requirements, this was not deemed as a serious obstacle in the preceding discussion. To improve the situation for the RANS grid and to avoid a possible pollution of the results, the mode shapes are re–defined to avoid extrapolation using CVT. The mode shapes are linearly extrapolated to the trailing edge line at each spanwise location (rib) of the finite–element model as a preprocessing step before they are applied in the intergrid transfer formulation in the CFD solver.

The influence of this mode shape modification on the Euler results is analysed shortly. Euler kriging results are shown in Fig. 18(b) with the kriging reference solution taken from Fig. 3. Results of the exact eigenvalue solver are not included at this point as excellent agreement was demonstrated above. The results denoted "new mode shapes" use the second frequency domain extraction approach for the re–defined mode shapes. Clear differences compared with the reference results can be found around the bucket of shock induced limit–cycle oscillation (LCO) bringing the current results closer to the prediction in [38]. This can be explained by the effects of the improved mode shapes. It was found that the extrapolation using CVT does not significantly pollute the intergrid transformation for the first mode which has a dominant bending behaviour. The first mode is the unstable mode in the lower Mach number range where the differences to the reference solution are small. The differences to the results in [38] are small but distinct and are not simply explained by the intergrid transformation. The three higher modes have a stronger torsional character with the CVT transformation giving poorer results when extrapolating to the trailing edge. The dynamics in the LCO bucket are dominated by the second mode (dominant torsion) which could explain the differences to the reference solution using the original mode shapes. The results indicate two points. First, the numerical implementation of an intergrid transfer method (such as CVT) is important and can result in uncertainty for the stability prediction as presented in [44]. Secondly, the mode shapes themselves are important. As these depend on the structural model, variability in the structural model parameters should be considered routinely. This latter issue was previously investigated in [22] for the Goland wing.

As a frequency domain solver to extract the samples of the Schur interaction matrix is currently not available for the RANS equations, forced time domain simulations are required. The response signals of the generalised forces are analysed directly to evaluate the interaction matrix (i.e. the aerodynamic influence coefficient matrix). For each numerical sample, four unsteady simulations are required for the four retained normal modes exciting one mode at a time. Three cycles of motion with 50 real time steps per cycle are used which allows the decay of startup transients to use the third cycle to extract the response information from the generalised forces. The excitation amplitude of the sinusoidal motion is defined to be 1.0×10^{-3}. At each real time step the solution is converged in pseudo time two orders of magnitude in about 10 to 20 pseudo iterations. The computational requirements for the RANS flow model are more demanding and the

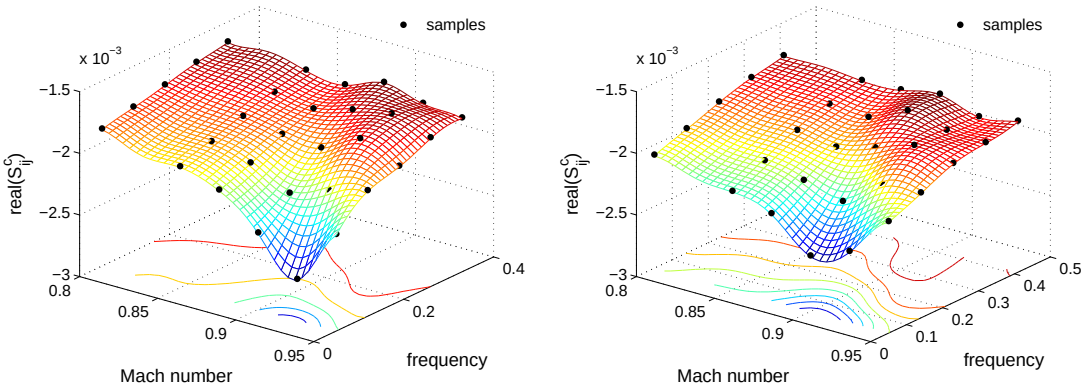

(a) Euler – real part

(b) coarse grid RANS – real part

Figure 19. Extracted and interpolated element real($S^c_{5,2}$) of Schur interaction matrix for Goland wing/store configuration using alternative extraction approach for Euler and RANS flow models.

need to run time domain simulations to extract the samples makes this situation worse. Using the coarser RANS grid, one steady state solution is simulated by converging the residual six orders of magnitude in about half an hour running on 16 processors. To extract one sample of the interaction matrix, requiring four unsteady runs as described in the previous paragraph, corresponds to about eight steady state solves. Using the finer RANS grid, the simulation of a steady state running on 32 processors takes about six hours, while the extraction of one sample then corresponds to two steady state simulations. To compare, a steady state solution for the Euler equations using a grid with 200 thousand control volumes is obtained in less than half an hour running on four processors with the extraction of one sample in the frequency domain taking less than one third of this time.

In Figs. 19(b) and 20 the results for coarse grid RANS simulations are presented. The response surface of one representative element of the Schur interaction matrix is shown in Fig. 19(b). The similarity to the Euler results in Fig. 19(a) is evident and expected. Within the considered range of freestream Mach numbers up to 0.95, shock induced flow separation is not yet encountered in the steady state RANS simulations, leaving the shock nonlinearity as the dominant mechanism of the dynamic response. Note that the differences found in typical flow characteristics such as surface pressure distributions (indicated in Fig. 18(a)) or skin friction (not shown herein) between the steady state RANS simulations using the coarser and finer grids are rather small indicating that the spatial resolution achieved by the coarser grid is acceptable. Figure 20 presents the corresponding results of the stability analysis. The figure indicates the instability points at fixed sea level conditions for all four aeroelastic modes originating in the wind–off structural modes. Critical values of the freestream velocity and the dimensionless frequency are given for the RANS simulations and compared with the Euler results. The configuration is unstable at a given Mach number once the instability boundary is first crossed with increasing freestream velocity.

The Euler results show the earlier discussed behaviour. At the lower Mach numbers the first mode is critical, developing the typical transonic dip, followed by the bucket of shock induced LCO. Also visible in the figure is the third mode instability dominating the response in the peak following the transonic dip at a freestream Mach number of about 0.9. The RANS results, using the coarser grid, show a surprising behaviour for the lower Mach numbers. While the second, third and fourth mode instabilities follow closely the Euler results, the first mode behaviour is significantly influenced. The RANS prediction, based on the kriging–reconstructed interaction matrix in Fig. 19(b), suggests that the second mode is critical over a larger range of Mach numbers below the transonic flow region followed by the first mode near the peak. The corresponding frequencies however are not effected by this switching of modes. The difference in the critical velocity is considerable even though a significant influence of the viscous effects would only be expected in the higher Mach number range due to the stronger shock/boundary layer interaction.

To investigate this behaviour in more detail, RANS simulations on the finer grid are included. Four samples, covering the first and second mode instabilities, are used initially with their locations in the parameter space indicated in Fig. 20(b). Then, the set of the four expensive RANS samples is augmented by the corner samples (limiting the parameter space) from a less expensive flow model. Here, cheaper samples from both

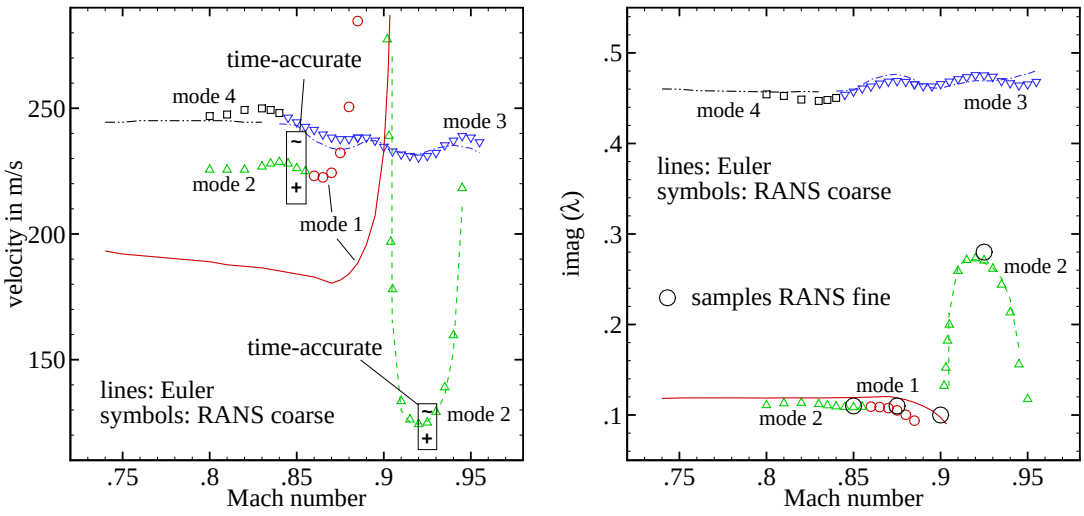

(a) Critical velocity

(b) Critical frequency

Figure 20. Instability behaviour of Goland wing/store configuration for Euler and RANS flow models showing critical values of velocity and dimensionless frequency at sea level conditions.

the Euler and the coarser grid RANS simulations are considered. Also, for the co–kriging approach the input parameter space of the augmented set of samples is extended by the response of the lower fidelity predictions to provide the trend information. Note that the step of using the results of RANS simulations on a coarser grid is important. The basic assumption of the co–kriging approach is the correlation in the parameter space between the responses of flow simulations having a variable fidelity. This variable fidelity can be established by using both different levels of the aerodynamic hierarchy and computational grids of different resolution. Exploiting the aerodynamic hierarchy requires that the dominant physics are captured by the chosen model. In the case of the Goland wing at zero degrees angle of attack, freestream Mach numbers below 0.95, and a reference Reynolds number of 15 million, shock induced flow separation was not predicted in the steady state simulations. This suggests that the shock dynamics are the driving mechanism which would allow the use of the Euler equations. If separation is encountered, then RANS simulations (or a lower fidelity model accounting for viscous effects) are required.

The results for the co–kriging approach are presented in Fig. 21. The figure shows the instability boundary given by the first and second mode obtained from the co–kriging approach based on both the Euler and coarser grid RANS results acting as the correlated co–variable to provide the trend information for the few more expensive samples. There are several interesting observations. First, in contrast to the results of the coarser grid RANS predictions, the lower range of Mach numbers is dominated by a bending–torsion type of instability, as expected, with the first mode being critical throughout. Secondly, the differences between the finer grid RANS and Euler predictions in the region of the bending–torsion type instability, forming the typical transonic dip, are smaller giving a similar behaviour compared with the aerofoil results [24]. The viscous effects have a stabilising influence on the configuration and increase the flutter onset velocity. Thirdly, for freestream Mach numbers below 0.85 the high fidelity predictions based on co–kriging using the Euler and coarser grid RANS results as correlated co–variables deviate considerably. This is due to the required extrapolation of the finer grid RANS response with the first initial sample being located at Mach 0.85 as shown in Fig. 20. Thus, below the freestream Mach number of 0.85 the predictions consequently either approach the Euler or coarser grid RANS results. Therefore, extrapolation should be avoided by a careful placement of the expensive high fidelity samples. Using an additional sample located at Mach 0.82, this latter observation is supported by the stability results as indicated in the figure. And finally, the critical freestream velocity in the bucket of shock induced LCO is increased by the RANS predictions using the finer grid compared with the lower fidelity results. Adding a second RANS sample using the finer grid at Mach 0.925 shows a further increase in the critical velocity.

Time–accurate simulations have been done to confirm the Euler and coarser grid RANS predictions. As with all time–accurate aeroelastic simulations in this study, the system parameters have been chosen following

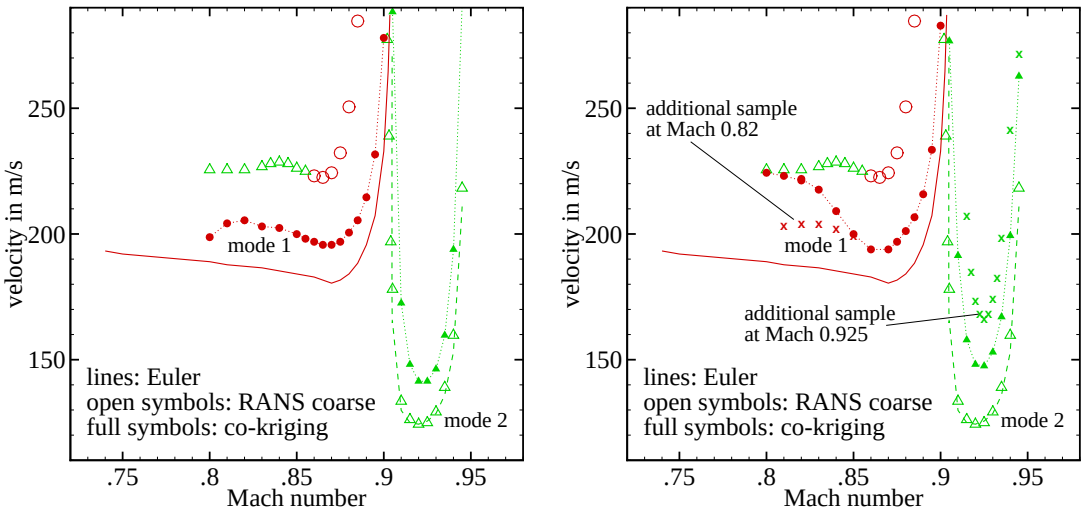

(a) Co–kriging based in Euler

(b) Co–kriging based on RANS (coarse)

Figure 21. Co–kriging technique applied to Goland wing/store configuration using both Euler and coarser grid RANS predictions as correlated co–variable.

the results of the eigenvalue–based linear stability analysis to avoid unnecessary iteration to bracket the instability. The RANS results are included in Fig. 20 with a plus (tilde) sign indicating a stable (unstable) response due to an initial disturbance in the structural unknowns. To give an idea of the computational cost involved for unsteady RANS flow modelling on the coarser grid, the simulation of one cycle of motion, requiring about 600 real time steps at a dimensionless response frequency of about 0.1 corresponding to a first mode instability and using a dimensionless time increment of 0.1, takes about six hours running on ten processors. Several cycles always have to be simulated following an initial excitation.

V. Conclusions

The aeroelastic stability analysis based on nonlinear computational fluid dynamics was investigated for the modal structural model to describe realistic aircraft structures. Particularly, the search for aeroelastic instability over a proposed transonic flight envelope, while exploiting the hierarchy of flow models, was addressed. This was demonstrated successfully by introducing searches for the approximation of the interaction matrix, modelling the influence of the high dimensional computational fluid dynamics system on the modified structural eigenvalue problem solved for the stability analysis. The approximation used the kriging interpolation technique based on exact numerical samples describing the system response. The co–kriging approach was formulated to allow the correction of a lower fidelity prediction with higher fidelity simulations guided by the lower fidelity results. Several aircraft structures were discussed including the aeroelastic configurations of the Goland wing, the MDO wing and the open source fighter.

Using kriging interpolation based on exact numerical samples to approximate the influence of the aerodynamics makes the approach essentially a model reduction technique. While the basic Schur complement eigenvalue method is faster than common time–accurate approaches, the reduced formulation proves to be computationally more efficient despite the cost invested in the construction of the kriging model itself. The construction of the kriging model using coordinated risk–based sampling to locate new sample locations iteratively makes the approach efficient in detecting aeroelastic instability in larger parameter spaces requiring not more than the cost of several steady state simulations.

Acknowledgments

This research forms part of the programme of the Marie Curie Excellence Team “Ecerta” financially supported by the European Union under contract MEXT–CT–2006–042383.

References

[1]Hassig, H. J., "An approximate true damping solution of the flutter equation by determinant iteration," *Journal of Aircraft*, Vol. 8, No. 11, 1971, pp. 885–889.

[2]Albano, E. and Rodden, W. P., "A doublet–lattice method for calculating lift distributions on oscillating surfaces in subsonic flows," *AIAA Journal*, Vol. 7, No. 2, 1969, pp. 279–285.

[3]Palacios, R., Climent, H., Karlsson, A., and Winzell, B., "Assessment of strategies for correcting linear unsteady aerodynamics using CFD or experimental results," *IFASD 2001–074*, 2001.

[4]Yurkovich, R. N., "Status of unsteady aerodynamic prediction for flutter of high–performance aircraft," *Journal of Aircraft*, Vol. 40, No. 5, 2003, pp. 832–842.

[5]Ashley, H., "Role of shocks in the "sub–transonic" flutter phenomenon," *Journal of Aircraft*, Vol. 17, No. 3, 1980, pp. 187–197.

[6]Shang, J. S., "Three decades of accomplishments in computational fluid dynamics," *Progress in Aerospace Sciences*, Vol. 40, 2004, pp. 173–197.

[7]Farhat, C., Geuzaine, P., and Brown, G., "Application of a three–field nonlinear fluid–structure formulation to the prediction of the aeroelastic parameters of an F–16 fighter," *Computers & Fluids*, Vol. 32, No. 1, 2003, pp. 3–29.

[8]Woodgate, M. A., Badcock, K. J., Rampurawala, A. M., Richards, B. R., Nardini, D., and deC Henshaw, M. J., "Aeroelastic calculations for the Hawk aircraft using the Euler equations," *AIAA Journal*, Vol. 42, No. 4, 2005, pp. 1005–1012.

[9]Romanowski, M. C., "Reduced order unsteady aerodynamics and aeroelastic models using Karhunen–Loeve eigenmodes," *AIAA Paper 96–3981*, 1996.

[10]Hall, K. C., Thomas, J. P., and Dowell, E. H., "Proper orthogonal decomposition technique for transonic unsteady aerodynamic flows," *AIAA Journal*, Vol. 38, No. 10, 2000, pp. 1853–1862.

[11]Lieu, T., Farhat, C., and Lesoinne, M., "Reduced–order fluid/structure modeling of a complete aircraft configuration," *Comput. Methods Appl. Mech. Engrg.*, Vol. 195, 2006, pp. 5730–5742.

[12]Lucia, D. J., Beran, P. S., and Silva, W. A., "Reduced–order modeling: new approaches for computational physics," *Progress in Aerospace Sciences*, Vol. 40, 2004, pp. 51–117.

[13]Silva, W. A. and Bartels, R. E., "Development of reduced–order models for aeroelastic analysis and flutter prediction using the CFL3Dv6.0 code," *Journal of Fluids and Structures*, Vol. 19, 2004, pp. 729–745.

[14]Hall, K. C., Thomas, J. P., and Clark, W. S., "Computation of unsteady nonlinear flows in cascades using a harmonic balance technique," *AIAA Journal*, Vol. 40, No. 5, 2002, pp. 879–886.

[15]Woodgate, M. A. and Badcock, K. J., "Implicit harmonic balance solver for transonic flow with forced motions," *AIAA Journal*, Vol. 47, No. 4, 2009, pp. 893–901.

[16]Morton, S. A. and Beran, P. S., "Hopf bifurcation analysis applied to deforming airfoils at transonic speeds," *AIAA Paper 97–1772*, 1997.

[17]Morton, S. A. and Beran, P. S., "Hopf–bifurcation analysis of airfoil flutter at transonic speeds," *Journal of Aircraft*, Vol. 36, No. 2, 1999, pp. 421–429.

[18]Badcock, K. J., Woodgate, M. A., and Richards, B. E., "Hopf bifurcation calculations for a symmetric airfoil in transonic flow," *AIAA Journal*, Vol. 42, No. 5, 2004, pp. 883–892.

[19]Badcock, K. J., Woodgate, M. A., and Richards, B. E., "Direct aeroelastic bifurcation analysis of a symmetric wing based on Euler equations," *Journal of Aircraft*, Vol. 42, No. 3, 2005, pp. 731–737.

[20]Woodgate, M. A. and Badcock, K. J., "Fast prediction of transonic aeroelastic stability and limit cycles," *AIAA Journal*, Vol. 45, No. 6, 2007, pp. 1370–1381.

[21]Badcock, K. J. and Woodgate, M. A., "Bifurcation prediction of large–order aeroelastic models," *AIAA Journal*, Vol. 48, No. 6, 2010, pp. 1037–1046.

[22]Marques, S., Badcock, K. J., Khodaparast, H. H., and Mottershead, J. E., "CFD based aeroelastic stability predictions under the influence of structural variability," *AIAA Paper 2009–2324*, 2009, to appear in Journal of Aircraft.

[23]Marques, S., Badcock, K. J., Khodaparast, H. H., and Mottershead, J. E., "On how structural model variability influences transonic aeroelastic stability," *AIAA Paper 2010–3047*, 2010.

[24]Timme, S. and Badcock, K. J., "Searching for transonic aeroelastic instability using an aerodynamic model hierarchy," *AIAA Paper 2010–3048*, 2010.

[25]Timme, S., Rampurawala, A., and Badcock, K. J., "Applying interpolation techniques to search for transonic aeroelastic instability: ANN vs kriging," 2010, Presented at the RAeS Aerodynamics Conference 2010, Bristol, United Kingdom, 2010.

[26]Badcock, K. J., Richards, B. E., and Woodgate, M. A., "Elements of computational fluid dynamics on block structured grids using implicit solvers," *Progress in Aerospace Sciences*, Vol. 36, 2000, pp. 351–392.

[27]Osher, S. and Chakravarthy, S. R., "Upwind schemes and boundary conditions with applications to Euler equations in general geometries," *Journal of Computational Physics*, Vol. 50, 1983, pp. 447–481.

[28]van Leer, B., "Towards the ultimative conservative difference scheme. V. a second–order sequel to Godunov's method," *Journal of Computational Physics*, Vol. 32, 1979, pp. 101–136.

[29]Jameson, A., "Time dependent calculations using multigrid with applications to unsteady flows past airfoils and wings," *AIAA Paper 91–1596*, 1991.

[30]Goura, G. S. L., *Time marching analysis of flutter using computational fluid dynamics*, Ph.D. thesis, Department of Aerospace Engineering, University of Glasgow, Glasgow, United Kingdom, 2001.

[31]Badcock, K. J. and Woodgate, M. A., "Prediction of bifurcation onset of large order aeroelastic models," *AIAA Paper 2008–1820*, 2008.

[32]Bekas, C. and Saad, Y., "Computation of smallest eigenvalues using spectral schur complements," *SIAM J. Sci. Comput.*, Vol. 27, No. 2, 2005, pp. 458–481.

[33]Wright, J. R. and Cooper, J. E., *Introduction to aircraft aeroelasticity and loads*, John Wiley & Sons, Ltd, Chichester, England, 2007.

[34]Bakhle, M. A., Mahajan, A. J., Keith, Jr., T. G., and Stefko, G. L., "Cascade flutter analysis with transient response aerodynamics," *Computers & Structures*, Vol. 41, No. 5, 1991, pp. 1073–1085.

[35]Silva, W. A., "Simultaneous excitation of multiple–input/multiple–output CFD–based unsteady aerodynamic systems," *Journal of Aircraft*, Vol. 45, No. 4, 2008, pp. 1267–1274.

[36]Jones, D. R., Schonlau, M., and Welch, W. J., "Efficient global optimization of expensive black–box functions," *Journal of Global Optimization*, Vol. 13, No. 4, 1998, pp. 455–492.

[37]Sacks, J., Welch, W. J., Mitchell, T. J., and Wynn, H. P., "Design and analysis of computer experiments," *Statistical Science*, Vol. 4, No. 4, 1989, pp. 409–435.

[38]Beran, P. S., Khot, N. S., Eastep, F. E., Snyder, R. D., and Zweber, J. V., "Numerical analysis of store–induced limit–cycle oscillation," *Journal of Aircraft*, Vol. 41, No. 6, 2004, pp. 1315–1326.

[39]Rodden, W. P. and Johnson, E. H., *MSC.Nastran aeroelastic analysis user's guide*, MSC.Software Corporation, Santa Ana, CA, 2004.

[40]Badcock, K. J., Timme, S., and Marques, S., "Implementing the Schur complement eigenvalue formulation in the DLR TAU code," Tech. rep., Computational Fluid Dynamics Laboratory, University of Liverpool, Liverpool, United Kingdom, 2010.

[41]de C. Henshaw, M. J., Badcock, K. J., Vio, G. A., Allen, C. B., Chamberlain, J., Kaynes, I., Dimitriadis, G., Cooper, J. E., Woodgate, M. A., Rampurawala, A. M., Jones, D., Fenwick, C., Gaitonde, A. L., Taylor, N. V., Amor, D. S., Eccles, T. A., and Denley, C. J., "Non–linear aeroelastic prediction for aircraft applications," *Progress in Aerospace Sciences*, Vol. 43, 2007, pp. 65–137.

[42]Cattarius, J., *Numerical wing/store interaction analysis of a parametric F–16 wing*, Ph.D. thesis, Virginia Polytechnic Institute and State University, 1999.

[43]Cazier, Jr., F. W. and Kehoe, M. W., "Ground vibration test on an F–16 airplane with modified decoupler pylons," Tech. Rep. NASA–TM–87634, NASA Langley Research Center, Hampton, VA, 1986.

[44]Swift, A. and Badcock, K. J., "Inter–grid transfer influence on transonic flutter predictions," *AIAA Paper 2010–3049*, 2010.